Sedimentology (1990), **37**, 647–672

The variability of critical shear stress, friction angle, and grain protrusion in water-worked sediments

JAMES W. KIRCHNER*[1], WILLIAM E. DIETRICH†, FUJIKO ISEYA‡ *and* HIROSHI IKEDA‡

**Energy and Resources Group, and †Department of Geology and Geophysics, University of California, Berkeley, CA 94720, USA*

‡Environmental Research Center, University of Tsukuba, Ibaraki 305, Japan

ABSTRACT

The erodibility of a grain on a rough bed is controlled by, among other factors, its relative projection above the mean bed, its exposure relative to upstream grains, and its friction angle. Here we report direct measurements of friction angles, grain projection and exposure, and small-scale topographic structure on a variety of water-worked mixed-grain sediment surfaces. Using a simple analytical model of the force balance on individual grains, we calculate the distribution of critical shear stress for idealized spherical grains on the measured bed topography. The friction angle, projection, and exposure of single grain sizes vary widely from point to point within a given bed surface; the variability within a single surface often exceeds the difference between the mean values of disparate surfaces. As a result, the critical shear stress for a given grain size on a sediment surface is characterized by a probability distribution, rather than a single value. On a given bed, the crtitical shear stress distributions of different grain sizes have similar lower bounds, but above their lower tails they diverge rapidly, with smaller grains having substantially higher median critical shear stresses. Large numbers of fines, trapped within pockets on the bed or shielded by upstream grains, are effectively lost to the flow. Our calculations suggest that critical shear stress, as conventionally measured, is defined by the most erodible grains, entrained during transient shear stress excursions associated with the turbulent flow; this implies a physical basis for the indeterminacy of initial motion. These observations suggest that transport rate/shear stress relationships may be controlled, in part, by the increasing numbers of grains that become available for entrainment as mean shear stress increases. They also suggest that bed textures and grain size distributions may be controlled, within the constraints of an imposed shear stress and sediment supply regime, by the influence of each size fraction on the erodibility of other grain sizes present on the bed.

INTRODUCTION

Bedload transport rates are often predicted by comparing the imposed boundary shear stress to a reference critical shear stress, which represents the stress required for particle entrainment by the flow (e.g. du Boys, 1879; Shields, 1936; Meyer-Peter & Müller, 1948). This threshold stress is usually determined by extrapolation of a regression relationship between shear stress and transport rate or, in flume studies, by gradually increasing slope or water discharge until 'initial motion' of grains is first detected. Because turbulent flow produces stochastic stress fluctuations at the bed (Grass, 1971), the probability of grain motion has no definite cut-off, sampling variation makes the dependence of transport rate on stress vague in low-stress regimes, and the determination of transport threshold shear stresses is thus inherently subjective (e.g. Paintal, 1971; Wilcock & Southard, 1988). In practice, therefore, the threshold stress is sometimes replaced by a 'reference' stress at which some small, but finite, transport rate is observed

[1] Now at: Division of Geological and Planetary Sciences 170–25, California Institute of Technology, Pasadena, CA 91125, USA.

or predicted (Parker & Klingeman, 1982). However, whether a 'reference' or 'threshold' stress is taken to be the critical shear stress, relating that stress to measurable properties of the bed and bedload material remains a central problem in bedload transport mechanics.

The roughness of a stream bed varies from place to place within a given channel reach. Therefore, spatial variations in the local critical shear stress would be expected, in addition to temporal fluctuations in the instantaneous applied shear stress from turbulent flow.

Even within a uniformly rough portion of a stream bed, however, there may be point-to-point variation in the factors that control the critical shear stress of each individual grain. Indeed, such small-scale variation in surface properties is part of the disorder inherent in a rough surface. Such variability (among individual grains) implies that the critical shear stress for a collection of grains (representing any region of the bed) may not be well defined. Here we quantify, by direct measurement, this intrinsic variability for water-worked beds, and describe its consequences for the variability of critical shear stress.

Attempts to describe the physics of sediment transport inevitably lead to the problem of constructing a force balance for individual sediment grains on a rough bed (see Fig. 1). Two key elements of this force balance are (i) the friction angle Φ, also called the pivoting angle (Li & Komar, 1986) or angle of repose (Miller & Byrne, 1966), which expresses the resistance to removal of the grain by the flow, and (ii) the relative protrusion of the grain above the bed, which affects exposure to the flow (Fenton & Abbott, 1977). Some sediment transport theories recognize these factors explicitly, while others invoke them implicitly as components of 'hiding' functions. These variables are thought to affect not only the critical shear stress, but also the relative mobility and selective entrainment of different sediment size fractions (Parker & Klingeman, 1982; Komar & Li, 1986, 1988; Wiberg & Smith, 1987a), and the mechanics of bedload transport pulsations due to longitudinal sediment sorting (Iseya & Ikeda, 1987; Whiting *et al.*, 1988).

By inspection, it is clear that grain protrusion and friction angle will vary with the size, shape, and orientation of the individual grains, as well as the size, shape, orientation, and packing arrangement of the grains comprising the local bed surface (Fig. 1). Analytical predictions of friction angle and grain protrusion (from grain size data, for example) are

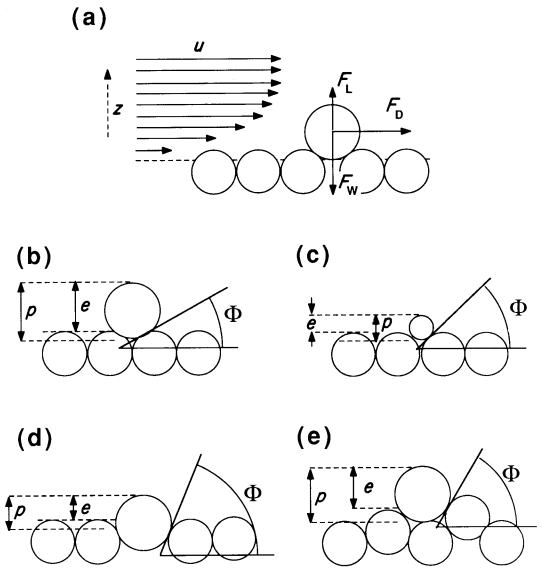

Fig. 1. (a) Force balance on a grain on a rough bed, where F_L, F_D, and F_W are the forces of lift, drag, and weight acting on the grain, u is the mean flow velocity, and z is the height above the local mean bed surface. (b, c, d, e) Variation of factors affecting force balance—friction angle (Φ), grain projection (p) above the local mean bed surface, and grain exposure (e) above the local upstream maximum bed surface—with the relative size (b, c) and packing arrangement (d, e) of grains.

therefore possible only for artificially simplified pocket geometries (such as regular packing arrangements of identical spheres) that may bear little resemblance to the bed textures observed in natural sediments. Consequently, for natural beds these variables must necessarily be characterized by empirical relationships derived from direct measurement.

Here we present, for the first time, measurements of friction angle and grain protrusion distributions for a variety of water-worked sediments. We also evaluate the implications of these distributions for critical shear stresses on water-worked beds. Such data should aid in selecting appropriate friction angle and protrusion values for physically based studies of sediment transport mechanics. A more complete understanding of the controls on the distribution of friction angle and protrusion (and, by implication, surface grain entrainability) in water-worked sediments should also assist in inferring flow and sediment supply conditions from sedimentary facies observed in the field.

Definitions of the mathematical symbols used in this paper are given in the Appendix.

METHODS

The measurements reported here were made as part of a flume study focusing on the relationship between sediment supply, boundary shear stress, and surface coarseness (Dietrich *et al.*, 1989). In three experimental runs, we progressively reduced the sediment feed rate to a small (0·3 m wide, 7·5 m long) flume, keeping the water discharge (0·6 $1\ s^{-1}\ cm^{-1}$), flume slope (0·26°), and sediment feed size distribution constant. The water surface slope, bed surface slope, and bed surface texture were allowed to equilibrate to the imposed water discharge and bedload supply rate (varied between runs: 17·4, 6·1, and $1·7\ g\ min^{-1}\ cm^{-1}$). Fresh sediment was fed continuously into the upstream end of the flume by hand or conveyor belt. Discharged bedload was collected from the flume outlet at 5-min intervals, weighed, and sieved to determine grain size distribution. The water suface and bed slope were determined every 6 min from point gauges at 1-m intervals along the flume centreline. Each run, lasting 6–8 h, was halted when the water surface slope stabilized and when the rate and size distribution of bedload discharge matched those of bedload supply, i.e. when approximate equilibrium was reached. The flow parameters at equilibrium are given in Table 1.

A poorly sorted mixture of natural sediment grains ranging from very coarse sand (1 mm) to medium gravel (12 mm, Corey shape factor 0·6–0·66) was used for both the bedload supply and the initial bed surface (for size distribution, see Table 2). All sediment was mixed and handled while damp to minimize settling of finer sediment between larger grains.

Before the experiment began, a set of plywood boards (0·3 m wide, 0·5 m long) was buried in the flume bed, and covered with the same sediment mixture used for the initial bed and sediment feed. At the end of each run, the flume was drained and one or two boards were removed by excavating their edges, keeping the sediment on the boards intact. The boards were allowed to dry, and the undisturbed bed surface was then fixed with cyanoacrylate-based glue, chosen for its very low viscosity and surface tension. Because this glue did not fill the pore spaces between the grains, it fixed the bed surface without altering the surface texture; it even preserved much of the surface roughness of the individual grains.

Bed surfaces formed at three sediment transport rates ($17·4, 6·1$ and $1·7\ g\ min^{-1}\ cm^{-1}$) were preserved, as was a sample of the initial bed surface, after wetting but before any transport took place (hereafter referred to as the 'unworked bed'). At the highest transport rate, there was marked longitudinal sorting of the bed surface and bedload into features alternatively termed 'congested-smooth sequences' (Iseya & Ikeda, 1987) or 'bedload sheets' (Whiting *et al.*, 1988). The bed surface from this run was divided into congested (coarse), smooth (fine), and transitional (intermediate) zones, each of which was separately analysed; the average values for the high-transport-rate bed are the area-weighted average of measurements on these zones.

Grain size distributions of the bed surfaces (Table 2) were measured by the grid-by-number method (Wolman, 1954; Kellerhals & Bray, 1971). The preserved bed surfaces were mounted on a gear-driven x–y table, and a needle was mounted in a fixed frame overhead. Positioning the bed at a fixed grid of points, the single grain beneath the needle was measured with calipers. Between 200 and 300 grains were measured for each bed surface. Kellerhals & Bray's analysis

Table 1. Summary of equilibrium flow parameters.

	Bedload transport rate ($g\ min^{-1}\ cm^{-1}$)		
	17·4	6·1	1·7
Water discharge ($1\ s^{-1}\ cm^{-1}$)	0·60	0·60	0·60
Mean flow velocity ($cm\ s^{-1}$)	58	58	53
Mean flow depth (cm)	10·2	10·3	11·3
Water surface slope ($mm\ m^{-1}$)	5·2	4·6	3·5
Froude number	0·60	0·52	0·50
Boundary shear stress ($dyne\ cm^{-2}$)	53	47	39
Median bed surface grain diameter (mm)	3·74	4·26	4·85
Length of run (h)	7·5	7·5	6·0

Table 2. Bed surface grain size distributions at transport rates (g min^{-1} cm^{-1}) of: (a) 17·4, (b) 6·1, (c) 1·7.

	(a)				(b)	(c)		
	Surface type							
	Transitional	Smooth	Congested	Average			Unworked bed	Sediment feed
d (mm)								
1·4	30†	37	8	28	12	17	16	22
2	35	46	14	35	21	21	21	30
3	42	52	21	42	31	25	26	41
4	54	59	36	53	46	36	47	55
5	63	72	56	64	63	52	65	74
6	72	79	71	74	76	68	80	85
7	84	84	83	84	84	79	89	93
8	89	92	92	90	91	86	94	98·1
9	92	95	96	94	95	91	98·1	99·2
10	95	97	98	96	99·3	95	99·4	99·9
11	98·2	100	99·5	98·9	99·3	98·6	100	100
12	99·8	100	100	99·9	100	99·5	100	100
Percentile								
20	<1·40‡	<1·40	2·86	<1·40	1·92	1·83	1·94	<1·40
30	1·44	<1·40	3·59	1·54	2·90	3·43	3·19	1·97
40	2·70	1·66	4·19	2·69	3·61	4·23	3·68	2·94
50	3·68	2·65	4·71	3·74	4·26	4·85	4·19	3·63
60	4·70	4·09	5·28	4·63	4·85	5·49	4·74	4·24
70	5·78	4·86	5·91	5·58	5·57	6·20	5·35	4·78
80	6·67	6·13	6·73	6·61	6·54	7·18	5·99	5·53
90	8·43	7·76	7·78	7·99	7·91	8·76	7·24	6·60

† Percent finer.
‡ Diameter (mm).

indicates that these grid-by-number size distributions should be equivalent to the traditional sieve-by-weight distribution used to characterize the bedload.

To measure friction angles, we mounted the preserved bed surfaces in a rigid metal frame connected to reduction gearing which allowed us to tilt the bed surface slowly, smoothly and precisely, without vibration or backlash. Friction angles were measured for three sizes of test grains, chosen from the approximate D_{16}, D_{50}, and D_{84} of the sediment feed. We placed individual test grains on the horizontal bed by dropping them from 50 mm above it; in this way all areas of the bed were sampled, but the location and orientation of individual grains were randomized. We then tilted the bed until the test grain rotated or slid a distance of more than one grain diameter, and read the friction angle for that grain from an optical clinometer fixed to the tilting frame. We obtained the friction angle distributions (Table 3) by repeating this measurement 100 times for each of the 18 test grain/bed type combinations (three test grain sizes × six bed surfaces). We used the same collection of test grains for all the friction angle measurements. Preserved surfaces of the water-worked beds were not tilted beyond 90° due to concern for their physical integrity.

On two of the bed surfaces used for friction angle measurements (the congested and smooth zones from the 17·4-g-min^{-1}-cm^{-1} run), grain protrusion was estimated using microtopographic profiles measured along a streamwise transect. Mounting the preserved bed surface on a gear-driven x–y table, we measured the elevation of the surface (relative to an arbitrary datum) at 0·2-mm intervals (roughly one-fifth the diameter of the smallest grains) using a needle probe on a machinist's spring-loaded depth gauge mounted in a fixed frame overhead. Measurements and positioning were reproducible to within 0·02 mm in both the horizontal and vertical. Each transect covered approximately 0·2 m (about 20 times the diameter of the largest grains), and consisted of approximately 1000 individual elevation measurements. The profile measurement was designed to capture bed roughness at all scales, from the irregularities of individual grain surfaces to the form roughness of grain clusters.

We have not conducted an exhaustive set of experiments independently varying each of the parameters thought to affect friction angles and grain

Table 3. Bed surface friction angle distributions at transport rates (g min^{-1} cm^{-1}) of: (a) 17·4, (b) 6·1, (c) 1·7.

	(a)*				(b)	(c)		
	Surface type							
	Transitional	Smooth	Congested	Average			Unworked bed	Fine sandpaper
Percentile								
Large (5·66–6·73 mm diameter) test grains								
Φ_{10}	31†	25	33	30	33	33	38	22
Φ_{20}	37	31	37	36	41	37	42	30
Φ_{30}	43	37	41	41	44	41	47	32
Φ_{40}	47	41	44	45	51	45	51	36
Φ_{50}	51	46	48	49	53	49	56	39
Φ_{60}	56	49	55	54	57	54	60	41
Φ_{70}	62	52	59	59	61	60	67	45
Φ_{80}	68	58	69	65	67	64	74	49
Φ_{90}	75	65	76	74	75	77	87	53
Medium (3·36–4·00 mm diameter) test grains								
Φ_{10}	33	28	39	32	37	39	45	20
Φ_{20}	39	33	45	38	42	43	52	26
Φ_{30}	44	37	51	44	45	45	58	30
Φ_{40}	48	44	58	47	48	51	64	34
Φ_{50}	54	47	63	51	50	57	70	38
Φ_{60}	58	48	68	56	53	60	76	39
Φ_{70}	63	51	80	62	59	66	85	43
Φ_{80}	74	58	87	73	68	71	99	47
Φ_{90}	89	65	>90	88	79	86	>120	50
Small (1·19–1·41 mm diameter) test grains								
Φ_{10}	49	42	53	46	44	49	64	26
Φ_{20}	58	51	60	56	53	59	76	30
Φ_{30}	64	56	70	63	61	69	89	33
Φ_{40}	72	64	80	71	68	80	99	37
Φ_{50}	79	70	88	78	74	85	114	39
Φ_{60}	85	75	>90	84	88	>90	>120	43
Φ_{70}	>90	82	>90	>90	>90	>90	>120	45
Φ_{80}	>90	>90	>90	>90	>90	>90	>120	48
Φ_{90}	>90	>90	>90	>90	>90	>90	>120	53
Test grain size as percentile of bed size distribution:								
Large	K_{74}	K_{80}	K_{73}	K_{76}	K_{77}	K_{70}	K_{82}	
Medium	K_{50}	K_{57}	K_{31}	K_{49}	K_{41}	K_{33}	K_{40}	
Small	K_{22}	K_{27}	K_{06}	K_{21}	K_{09}	K_{13}	K_{12}	

† Friction angle (degrees).

protrusion (such as grain shape and size distribution, orientation, and packing geometry). Instead, by changing the sediment supply, we co-varied many of these parameters, as the surface became more or less armoured in response to supply changes. More comprehensive experiments would be needed for a complete description of the role of each of these factors in controlling friction angle and grain protrusion. Our major objective in this study, however, was not to predict friction angle and grain protrusion from each of their controlling parameters, but instead to estimate their variability, and its consequences for critical shear stress on natural sediments.

FRICTION ANGLES OF WATER-WORKED SEDIMENTS

Previous friction angle measurements

Friction angles have been measured for a variety of unworked surfaces (i.e. surfaces whose grains were arranged by various artificial means, rather than by the action of flowing water). Chepil (1959), adapting a method suggested by Shields (1936), measured the friction angle of closely sieved sands as follows: 'A uniform layer of sand of each sieve grade was cemented to a smooth metal plate. A thin layer of loose grains

from the same sieve grade was placed on top of the cemented layer of sand and the plate was tilted slowly until the first downward movement of individual grains became perceptible.' All investigators to date have used some variant of Chepil's measurement procedure. Chepil obtained a friction angle of 33°, which agrees well with Bagnold's (1941) conjecture that the friction angle should be similar to the mass angle of repose of a pile of grains. Note, however, that Chepil actually reported the approximate lower bound of the friction angles of a large sample of grains; the relationship of this lower bound to the friction angle of the majority of the grains is not obvious.

Eagleson & Dean (1961) measured friction angles for spheres of different sizes resting on two beds of uniform natural sands, one 1·83 mm in diameter and the other 0·79 mm in diameter. They showed that, as expected, the average friction angle (Φ) decreased with increasing D/K (where D and K are the diameters of the test grains and the bed particles, respectively), but that average values of Φ were 10–20° larger than theoretically expected from the geometry of a regular triangular packing of uniform spheres:

$$\tan \Phi = \frac{\gamma}{\sqrt{(D/K)^2 + 2(D/K) - 1/3}}, \qquad (1)$$

where γ ranges from $1/\sqrt{3}$ (when the test sphere pivots directly through the saddle between two bed spheres) to $2/\sqrt{3}$ (when the test sphere pivots directly over one of the bed spheres).

Miller & Byrne (1966) reproduced Eagleson & Dean's results for spherical test grains of different sizes resting on a bed of uniformly sized spheres. This implies that the angular bed grains used by Eagleson & Dean were not responsible for the departure from the theoretically expected relationship. Rather, it seems likely that the discrepancy results from irregular packing arrangements of the bed grains. By contrast, Φ values for spheres in the cannon-ball tetrahedron assumed by the geometric theory (Li & Komar, 1986) fall within a few degrees of those predicted by Eq. (1).

Miller & Byrne (1966) rejected the geometric approach to predicting Φ, and proposed instead that mean friction angles could be described by the empirical relationship

$$\bar{\Phi} = \alpha(D/\bar{K})^{-\beta}, \qquad (2)$$

where $\bar{\Phi}$ is the average friction angle in degrees, $\bar{K}$ is the average diameter of the bed grains, and the two parameters are fitted by regression. Fitting Eq. (2) to measurements on uniformly sized and poorly sorted beds of spheres, they observed that β increased with the degree of bed sorting (i.e. $\bar{\Phi}$ decreased more rapidly with $D/\bar{K}$ on a uniformly sized bed than on a poorly sorted one), while α was relatively insensitive to sorting. They also compared curves of $\bar{\Phi}$ vs. $D/\bar{K}$ for three beds of different grain shapes (spheres, nearshore sand, and crushed quartzite) and nearly identical size distributions, using typical bed particles as test grains. For these similarly sorted beds, they observed that values of α (and, therefore, of Φ) increased as sphericity and roundness decreased, while β was insensitive to grain shape. Accordingly, Miller & Byrne refer to α as the shape–roundness parameter and β as the sorting parameter.

Measurements by Li & Komar (1986) further illustrate the influence of grain shape on friction angle. Carefully controlling the pocket geometry of pebbles that 'closely approximated triaxial ellipsoids', they observed that Φ and α increased systematically with pebble flatness (i.e. with decreases in D_c/D_b, the ratio of the smallest and intermediate axial diameters), which controls the test grain's ability to roll. For $D_c/D_b > 0{\cdot}8$, the test grain always rolled out of its pocket, while for $D_c/D_b < 0{\cdot}6$, the test grain almost always slid from its pocket (Figs 6 & 7 of Li & Komar, 1986).

Li & Komar also found that imbricated beds of flat ($D_c/D_b \approx 0{\cdot}4$) ellipsoidal pebbles (in which the bed pebbles dipped upstream by 23°) had friction angles 20–25° greater than those of non-imbricated beds (in which the pebbles were laid flat). Imbricated ellipsoidal beds had Φ and α values even higher than those of highly angular crushed basalts, clearly illustrating the impact of grain packing on friction angle.

The measurements performed to date have demonstrated that friction angle is affected by many factors, including relative grain size (D/K), grain shape, and bed grain packing. These data do not, however, shed much light on a question more pertinent to interpreting both field and flume data, i.e. what friction angles can be expected *for natural sediments*, rather than for artificially constructed beds? The spatially variable surface of a natural sediment should be characterized by a (potentially wide) distribution of friction angles rather than the single values of Φ obtained for the artificial surfaces used in previous studies. It is less intuitively obvious, but nevertheless demonstrable, that beds of grains transported and deposited by turbulent fluid flows (as in natural rivers and experimental flumes) will have friction angles different from those of a bed formed by randomly mixing the same grains. The importance of such factors as bed grain packing geometry suggests that it will be difficult to

predict friction angles directly from simple descriptors such as grain shape and size distributions.

Comparison of water-worked and unworked beds

Because all previous friction angle measurements have been made on unworked beds, while natural sediment surfaces are water-worked, it is appropriate to ask whether comparable unworked and water-worked beds have similar friction angle properties. Some of our measurements can shed light on this question. As mentioned above, we preserved a sample of an unworked bed (which was formed by screeding and wetting the sediment mixture, but without allowing transport to take place). By coincidence, this unworked bed has nearly the same grain size distribution as that of the water-worked bed formed at the intermediate transport rate of 6·1 g min^{-1} cm^{-1} (Fig. 2a). The unworked bed is slightly better sorted, but the median grain sizes are indistinguishable within error (Table 2).

Note, however, that the friction angle distributions of the two surfaces are quite different. Friction angles measured on the unworked bed are consistently greater than those for the water-worked bed, and the differences increase with decreasing test grain size (Fig. 2b, c, d). For example, the difference in median friction angle between the two surfaces is only 3° for large test grains, but 20° for medium and 40° for small test grains. These results suggest that earlier friction angle measurements on unworked surfaces may not be directly applicable to natural water-worked sediments.

The difference in friction angles between the unworked and water-worked surfaces must result, in this case, not from a difference in grain size distribution or grain shape, but from a difference in grain packing geometry. Visual inspection of the two surfaces suggests that the unworked bed has a looser packing arrangement, with many pore spaces large enough to trap medium and small test grains. Of course, during sediment transport such pores will trap

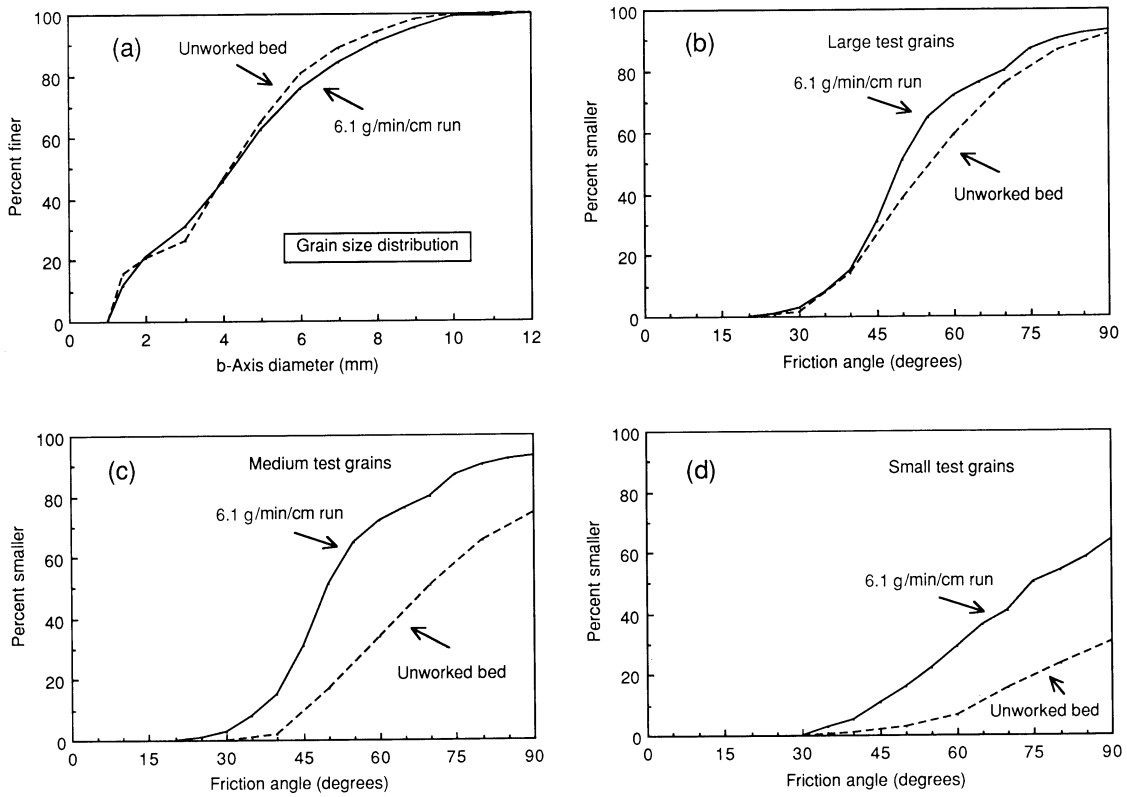

Fig. 2. Comparison of grain size distribution (a) and friction angle distributions (b, c, d) for an unworked bed and the water-worked bed from the 6·1 g $min^{-1}cm^{-1}$ run.

those grains, and thus close themselves and smooth the surface, decreasing its friction angles.

Friction angle and grain size, shape, and sorting

The median friction angles measured in this study show a power-law dependence on the ratio of test grain size to median bed grain size (Fig. 3), as described by Eq. (2) and observed by previous investigators. The fitted parameters α and β for Eq. (2) derived in this study are comparable to those obtained in previous studies (see Table 4).

The fitted parameters in Table 4, however, call into question Miller & Byrne's characterization of α and β in Eq. (2) as a shape parameter and sorting parameter, respectively. There is no correlation between bed grain size sorting and fitted values of β across the studies to date, nor any consistent relationship between α and grain shape. In particular, our comparison of unworked and water-worked beds suggests that even when grain shape and sorting are held constant, differences in packing geometry can create sizeable differences in both α and β values. There may be a relationship between α, β, shape, and sorting that is obscured by the comparison across different investigators presented here. If so, tightly controlled experiments should reveal that relationship. However, when Li & Komar controlled for both packing geometry and sorting, they found that grains

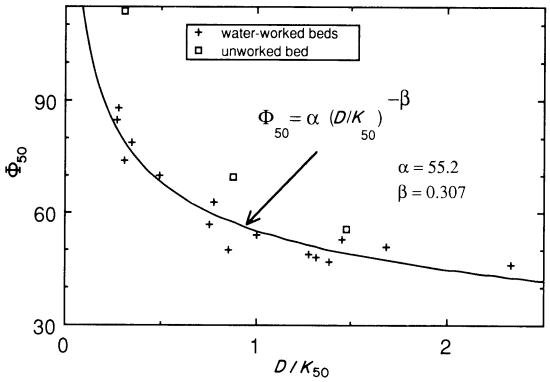

Fig. 3. Median friction angle (Φ_{50}) as a function of test grain diameter (D) and median bed grain diameter (K_{50}) for five water-worked beds. Data from unworked bed (see text) shown for comparison.

Table 4. Regression coefficients for equation 2 reported by various investigators.

Investigator and bed type	$\bar{\Phi}=\alpha(D/\bar{K})^{-\beta}$		
	α	β	r^2
Irregular bed grain packing			
Miller & Byrne (1971)			
Poorly sorted subangular crushed quartzite, unworked	63·8	0·28	0·96
Poorly sorted rounded natural sand, unworked	57·3	0·30	0·98
Poorly sorted glass spheres, unworked	45·7	0·32	0·91
Well-sorted glass spheres, unworked	44·9	0·44	0·99
Li & Komar (1986)			
Well-sorted, very angular crushed basalt, unworked	51·3	0·33	0·98
Present study			
Poorly sorted, rounded to angular, water-worked	55·2	0·31	0·91
Poorly sorted, rounded to angular, unworked	66·1	0·46	0·99
Controlled bed grain packing (tetragonal, saddle rotation)			
Li & Komar (1986)			
Well-sorted spheres	20·4	0·75	0·99
Well-sorted ellipsoidal pebbles	31·9	0·36	0·87

In all studies reported here, test grains were similar in shape to bed grains. Coefficients for Miller & Byrne's poorly sorted beds derived by our transformation of their $\bar{K}$ to the median bed grain size, for direct comparison to our data. The mean bed grain size reported by Miller & Byrne weights the diameter of each grain equally, i.e. it is the mean by number of grains, which, for their poorly sorted sediments, is substantially smaller than the mean or median by weight. Li & Komar's (1986) and Wiberg & Smith's (1987a) treatments of Miller & Byrne's results fail to take account of this discrepancy. We use median friction angle for $\bar{\Phi}$ because we could not measure exact values over 90°, and thus could not include them in averages. The other authors use mean friction angle for $\bar{\Phi}$, and do not disclose whether they include or exclude friction angle measurements beyond 90° in this average.

of different shape (spheres and smooth ellipsoidal pebbles) had different values of β as well as α.

Distribution of friction angles

Exclusive emphasis on the mean or median friction angle (as in Fig. 3, Table 4, and previous studies) obscures two potentially important points that are made obvious by inspection of Fig. 2 and Table 3. First, a water-worked mixed-grain surface is characterized not by a single friction angle, but by a wide distribution of friction angles. Replicate measurements for a given test grain/bed surface combination typically span a range of 40–60°. This distribution may result from local variability in bed pocket geometry and from variation in the shape and orientation of individual test grains. However, it is precisely this sort of variability that bedload grains may be expected to encounter as they travel over a rough bed.

Secondly, for test grains that are small in relation to the median bed grain size, sizeable fractions of the friction angle measurements exceed 90°. These fractions represent locations on the bed where small grains could become trapped until they are entrained by lift forces, by small-scale turbulent eddies within individual pockets, or by removal of the grains that form the pocket itself (thus altering the pocket geometry and friction angle). Grains in these pockets could be effectively lost to the flow for long periods.

The distribution of friction angles can be made explicit by plotting each fraction (10th percentile, 20th percentile, etc.) individually against the test grain size/bed grain size ratio, and by extending Eq. (2) to read

$$\Phi_n = \alpha_n (D/K_{50})^{-\beta_n}, \tag{3}$$

where Φ_n is the nth percentile friction angle, K_{50} is the median grain size of the bed, and α_n and β_n are fitted individually for each value of n (Fig. 4). A simple collapsed form of Eq. (3),

$$\Phi_n = (30 + 0{\cdot}5n)(D/K_{50})^{-0{\cdot}3}, \tag{4}$$

agrees well with the coefficients α_n and β_n shown in Fig. 4, for n between 10 and 70. Note that as the size of the test grain decreases in relation to the median grain size of the bed, not only does the median friction angle increase, but the fraction of friction angles above any particular threshold (for example, $\Phi = 90°$) increases rapidly (Fig. 4).

The typical range of variation in friction angle within a single bed can be directly inferred from Fig. 4. For example, for a test grain equal to the median bed grain size ($D/K_{50} = 1$), the regression lines for the

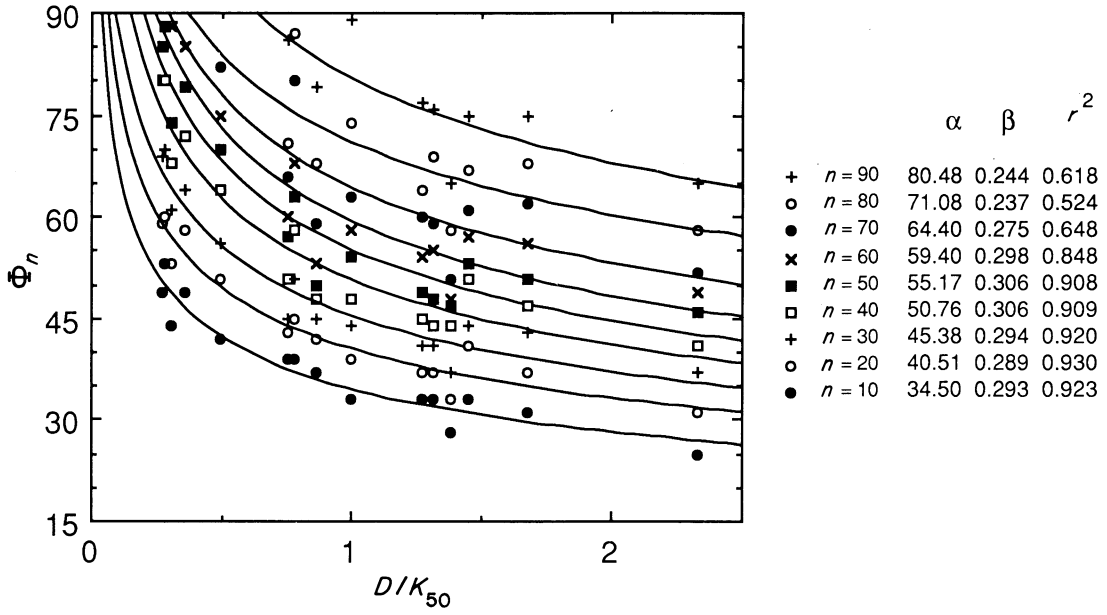

Fig. 4. Percentiles of friction angle distribution (Φ_n) as a function of test grain diameter (D) and median bed grain diameter (K_{50}) for five water-worked beds.

10th and 90th percentile friction angles span a range from 34 to 80°. If resistance to grain motion is roughly proportional to tan Φ (e.g. if the major motive force is simple fluid drag), then this range of friction angles represents an eightfold variation in the resistance to grain motion. For comparison, this range is three times greater than the range of variation in the median friction angle between the six water-worked beds in this study (7, 16, and 18°, respectively, for large, medium, and small grains).

How much friction angle variation is due to spatial variation in the bed itself, and how much results from the variable orientation and shape of individual rough grains? We have addressed this question empirically. First, we measured the friction angles for natural sediment grains on a given rough bed (here, the bed preserved from the 6·1-g-min^{-1}-cm^{-1} run). Next, we isolated the effect of bed roughness by measuring friction angles for glass spheres (in equivalent sieve sizes) on the same bed, thus eliminating test grain roughness, angularity, and variability as sources of friction angle variation. Finally, we isolated the effect of grain properties by measuring friction angles for the same natural grains on a flat non-slip surface (very fine, 600-mesh sandpaper), thus eliminating bed roughness and its variation. (This measurement also determines the limit that Φ should approach in the limit of large D/K_{50}. While Eq. (2) or (3) is useful as a purely empirical, descriptive relationship, extrapolation to high D/K for irregular grains may be misleading because Φ, rather than declining to zero, should instead converge to some non-zero value controlled by grain shape.) Note that the friction angle is not a simple sum of angles attributable to the bed and the test grain; likewise, the variation in friction angle need not be a sum of component variances.

As expected, because the spheres lack the natural grains' angularity, they have systematically lower friction angles on the rough bed (Fig. 5) . Similarly, natural grains have lower friction angles on a flat frictional surface than they do on a natural water-worked bed. Eliminating either grain roughness or surface roughness, however, only decreases the median friction angle by 10–15°. Furthermore, the variation in friction angle, as measured by the standard deviation of 100 replicate measurements, is comparably large whether it results from variability in the bed alone (15°), the test grains alone (12°), or both combined (14°). Friction angle variation, then, is not the sole result of either the variability in the bed or in the grains travelling over it; either is sufficient to produce the observed variation in friction angles.

We have characterized individual sediment beds by a distribution of friction angles, rather than a single mean value as in previous studies. This, however, is primarily a difference of emphasis, not of evidence. The standard deviations of our replicate measurements of friction angle for a given test grain/bed surface combination average approximately 17° over all such combinations. This is almost exactly the same as the standard deviations of Miller & Byrne's measurements. However, whereas they, and Li & Komar, have emphasized the differences *between* mean friction angles as a function of D/K, sorting, and angularity, we also recognize that for friction angles of natural sediments the variation *around* individual means is not simply a kind of measurement error to be averaged out. It instead reflects a physically realistic and mechanistically important variability in the resistance to grain transport within an individual bed surface.

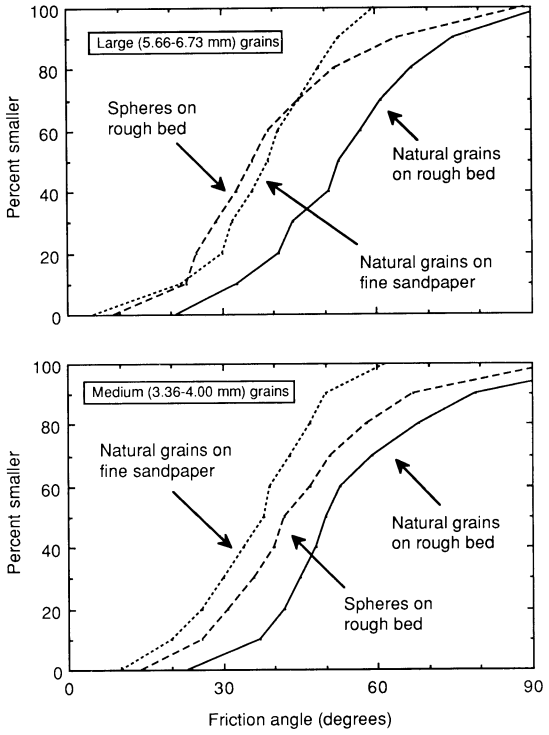

Fig. 5. Friction angle distributions for large and medium sediment grains on bed from the 6·1 g min^{-1}cm^{-1} run, similar-size spheres on the same bed surface, and sediment grains on a flat, frictional surface (600-mesh sandpaper).

SURFACE ROUGHNESS AND GRAIN PROTRUSION

The small-scale surface topography of a rough bed has obvious importance, not only for the distribution of friction angles on its surface, but also for grain protrusion, hydraulic roughness, and the detailed near-bed flow field. Direct measurement and quantitative characterization of bed surface topography have only recently been attempted (e.g. Furbish, 1987). Instead, bulk roughness properties of the bed (such as hydraulic roughness) have typically been indirectly inferred by their effects on fluid flow properties (such as the vertical profile of mean velocity). Empirical curve-fitting has then been used to relate the measured roughness to measurable bed parameters, such as grain size distribution. However, the direct effect of, for example, grain size distribution on the small-scale topographic structure of the bed surface and its effect, in turn, on hydraulic roughness, grain friction angles, and grain protrusion have remained largely unknown.

To discuss adequately, let alone resolve, each of these issues is far beyond the scope of this study. In particular, how the surface topography is controlled by grain packing on poorly sorted beds, and how that surface shapes the near-bed flow over individual grains, are issues on which we currently have little to offer. We will, however, present detailed topographic measurements for different beds, characterize the bed roughness statistically, and compare bed topography to measured and inferred friction angles and grain protrusion.

The bed surfaces analysed here are those of the congested and smooth zones from the bedload sheets formed during the 17·4-g-min^{-1}-cm^{-1} run described above. The congested zone is a relatively well-sorted jumble of coarse ($K_{50}=4{\cdot}7$ mm) grains with few fines to fill the pores between them ($K_{10}=2{\cdot}9$ mm). This zone is a distinct area of the bed that migrates downstream, and so is different in character from the isolated, static clast jams reported by Kuhnle & Southard (1988). The smooth zone has a somewhat finer surface ($K_{50}=2{\cdot}6$ mm) with isolated protruding large grains. The K_{90} grain sizes of both zones are very similar; the major grain size distinction between the two zones is the nearly complete absence of fines in the congested zone (Table 2). (In our nomenclature, in which D and K represent the diameters of the test grains and bed grains respectively, we use K_{50}, for example, where others use 'the D_{50} of the bed'.)

The topographic profiles (Fig. 6) clearly show the difference in granularity between the two surfaces. Note also that the congested zone is marked by many large, deep pockets between grains. Because of the way the profiles were constructed, they cannot show that these pockets often have overhanging walls and often connect to pore spaces beneath the surface grains, but this is in fact the case. These profiles can only approximate the three-dimensional structure of the bed.

It is clear that the surfaces revealed in these profiles bear little resemblance to the more orderly grain

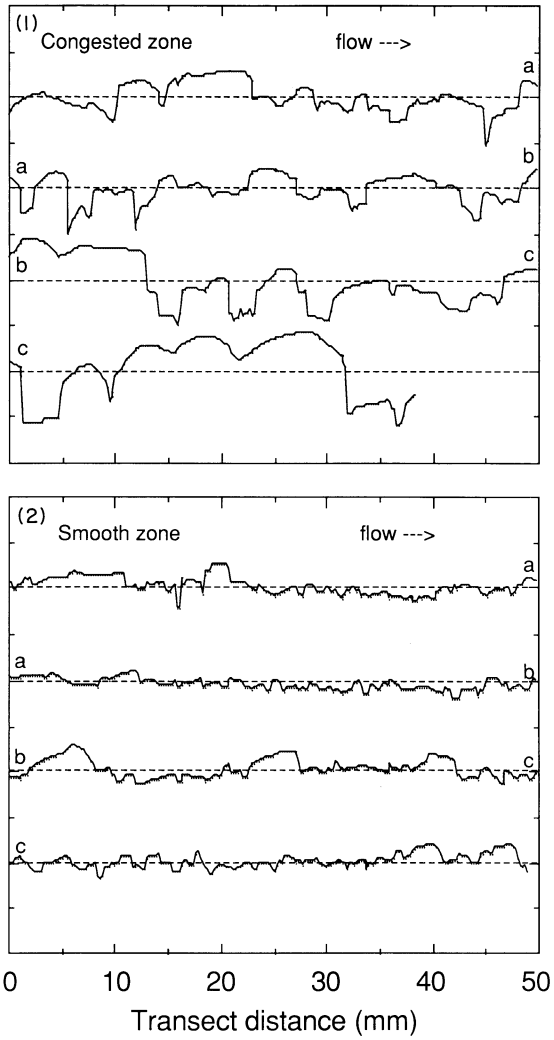

Fig. 6. Bed surface topography along streamwise transects for congested zone and smooth zone, 17·4 g min^{-1}cm^{-1} run. No vertical exaggeration. Flow is left to right. Transects are shown in wraparound; sections join at points marked a, b, and c. Dashed line shows level datum (mean bed surface).

arrangements typically shown in the sediment transport literature (e.g. Fig. 1), or the evenly spaced identical roughness elements usually assumed in the fluid dynamics literature. Of course, these simplifications are useful for many purposes; Fig. 6 simply illustrates how far they diverge from the complex structure present in actual sediment surfaces.

Statistics of sediment surfaces

Irregular, aperiodic surfaces such as shown in Fig. 6 must necessarily be characterized statistically. With the large number of individual elevation measurements contained in our profiles, we can measure the distribution of bed roughness as well as the overall vertical roughness scale (e.g. the standard deviation of elevation). The distributions of elevation and local slope (interpolated between adjacent points) for the two surfaces are shown in Fig. 7.

When grain packing geometries vary among surfaces, their roughnesses and grain size distributions may not be well correlated. Consider the two hypothetical bed surfaces, composed of a bimodal grain size distribution, shown in Fig. 8. The visibly rougher surface has, in fact, a *finer* surface grain size distribution but because its large grains protrude further, they create greater hydraulic roughness, as well as raising the small grains' friction angles and diminishing their exposure to the flow. There is little a priori reason to expect a one-to-one correspondence between bed surface topography and grain size distribution.

The profiles shown in Fig. 6 may be expected to have Gaussian distributions if, for example, they were

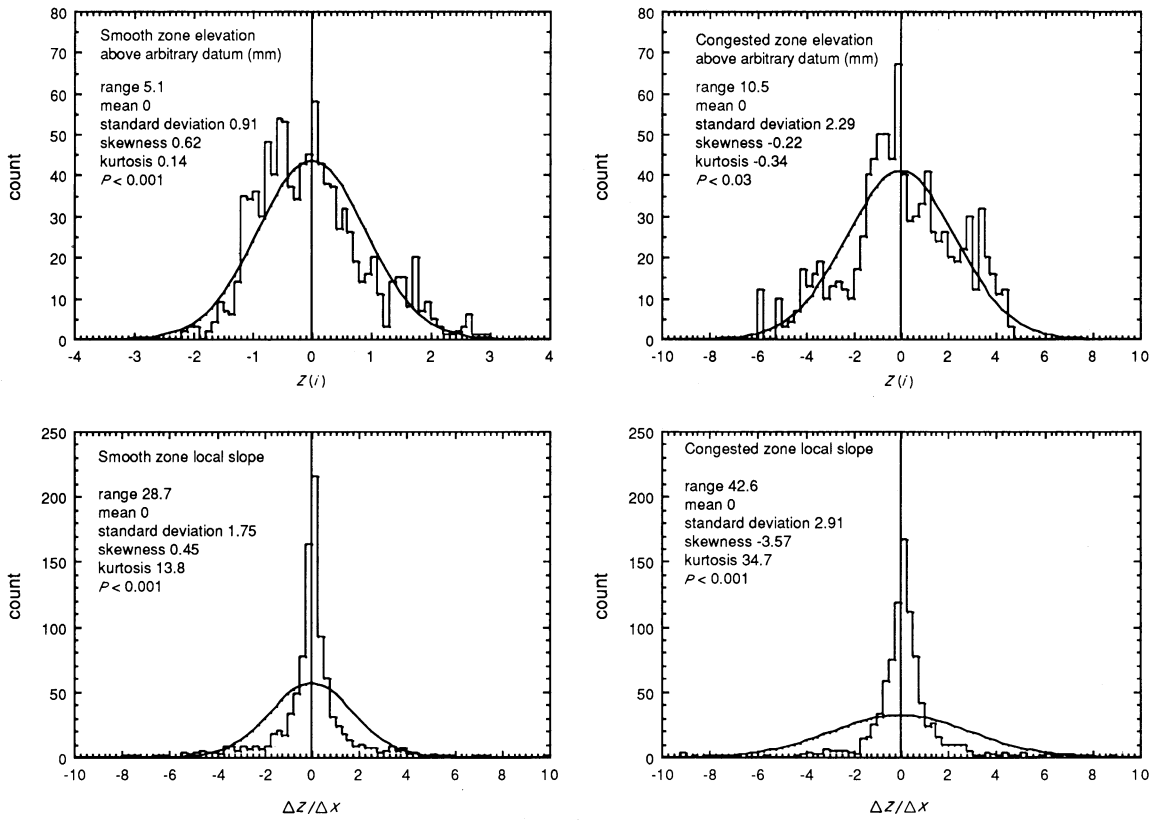

Fig. 7. Distribution of elevation and local slope, with descriptive statistics, for bed surface transects, with Gaussian (normal) distributions of equal mean and standard deviation for comparison. Measure of statistical significance (P) expresses likelihood, calculated by Kolmogorov–Smirnov D, that the observed distributions were sampled from Gaussian distributions shown. Standard errors of estimate of skewness and kurtosis are 0·08 and 0·16, respectively. Tick mark spacing on horizontal axis indicates width of cells into which measurements were tallied. Some extreme values on tails of local slope distributions are not shown.

approximated by a Brownian motion series (e.g. Furbish, 1987). While the individual elevation measurements are not overtly non-Gaussian, the local slope data are strongly leptokurtic, i.e. they have a cluster of values near the mean and very long tails (Fig. 7). These distributions statistically confirm what the transect profiles visually suggest: the profile roughness is 'squarer' than a Brownian motion trace would be, with steep transitions between plateaus. The elevation and local slope at any point are uncorrelated. The 'square' profile of the roughness may in part be an artefact of the way the measurement technique represents overhanging structures as vertical drops. However, the pattern persists in the smooth zone, where such overhangs are uncommon. Detailed measurement of the overhanging topography (as in a true cross-section of the bed) would shed additional light on the nature of the profiles, but would make analysis more difficult, as the profile would no longer be a single-valued function.

Grain protrusion and friction angle on bed profiles

To the extent that the bed surface profiles reflect the true bed surface topography, they can be used to create a proxy measure of grain protrusion and friction angles on the bed. Along the entire length of the enlarged transect profiles, discs (equal in diameter to the three test grain size classes) were placed at each point where these two-dimensional spherical 'grains' would come to rest (Fig. 9). The number of discs placed on each 20-cm profile varied with 'grain' size, from roughly 20 large discs to 60 small ones. We then measured the friction angle at the downstream point of contact, and the elevation of the top of the grain.

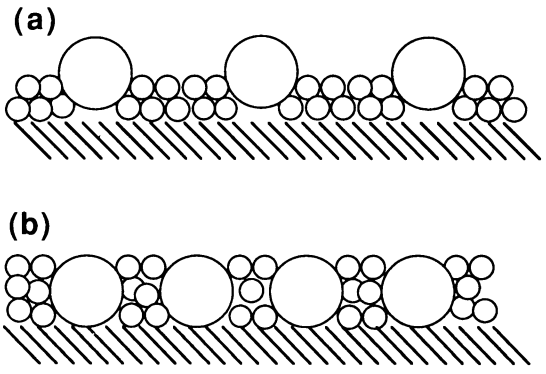

Fig. 8. Hypothetical bed cross-sections for bimodal grain size distribution. Bed (a) has greater roughness than (b), although its surface is finer.

Ideally, measures of grain protrusion should indicate how a grain's position on the bed affects its interaction with the flow. Two important factors are (i) the level of the grain with respect to the vertical velocity profile (here termed 'projection'), and (ii) the fraction of the grain not shielded by nearby upstream grains and therefore affected by the flow (here termed 'exposure') (Fig. 1). Grain projection is measured by the elevation of the top of the grain above the local mean bed surface elevation, here taken as the average elevation within a distance of K_{84} on each side of the grain's centre, which is also assumed as the reference height of the local logarithmic velocity profile (see below). We measure exposure by the elevation of the top of the grain above the local upstream maximum bed elevation, here taken as the highest bed elevation within a distance of K_{84} upstream of the grain's leading edge. These measures of protrusion and exposure were chosen because they are precisely defined (and therefore reproducible), and because K_{84} has been observed to be correlated with hydraulic roughness properties of mixed-grain beds (Leopold, Wolman & Miller, 1964). Defining more mechanistically realistic measures of grain protrusion must await

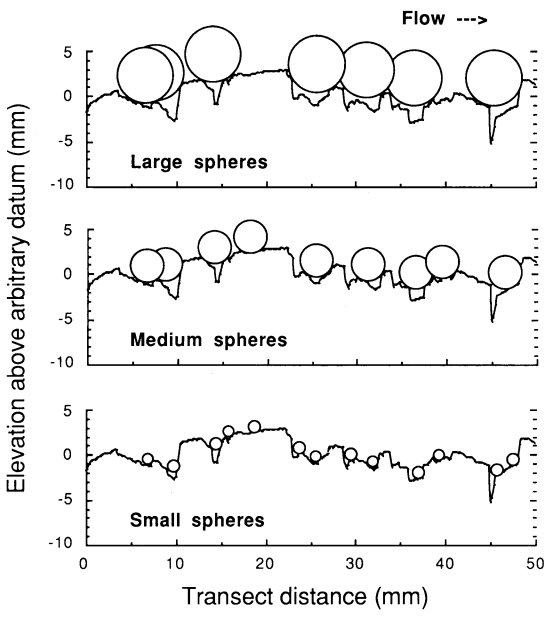

Fig. 9. Sample placement of circular discs, representing three sizes of idealized, spherical test grains, on bed surface transect profiles to estimate friction angle and grain protrusion distributions. Only 5 cm of the congested transect is shown; grain protrusion and friction angle distributions were estimated from the full length of each transect.

a more detailed understanding of the turbulent flow field near rough boundaries.

Friction angle distributions estimated from the transect elevation profiles are comparable to those measured by tilting with natural grains, but there are explainable systematic differences (Fig. 10). Friction angles estimated from the profile are generally smaller than measured friction angles, and the discrepancy is more marked on the congested zone. At least two factors may account for this. First, the disc-shaped

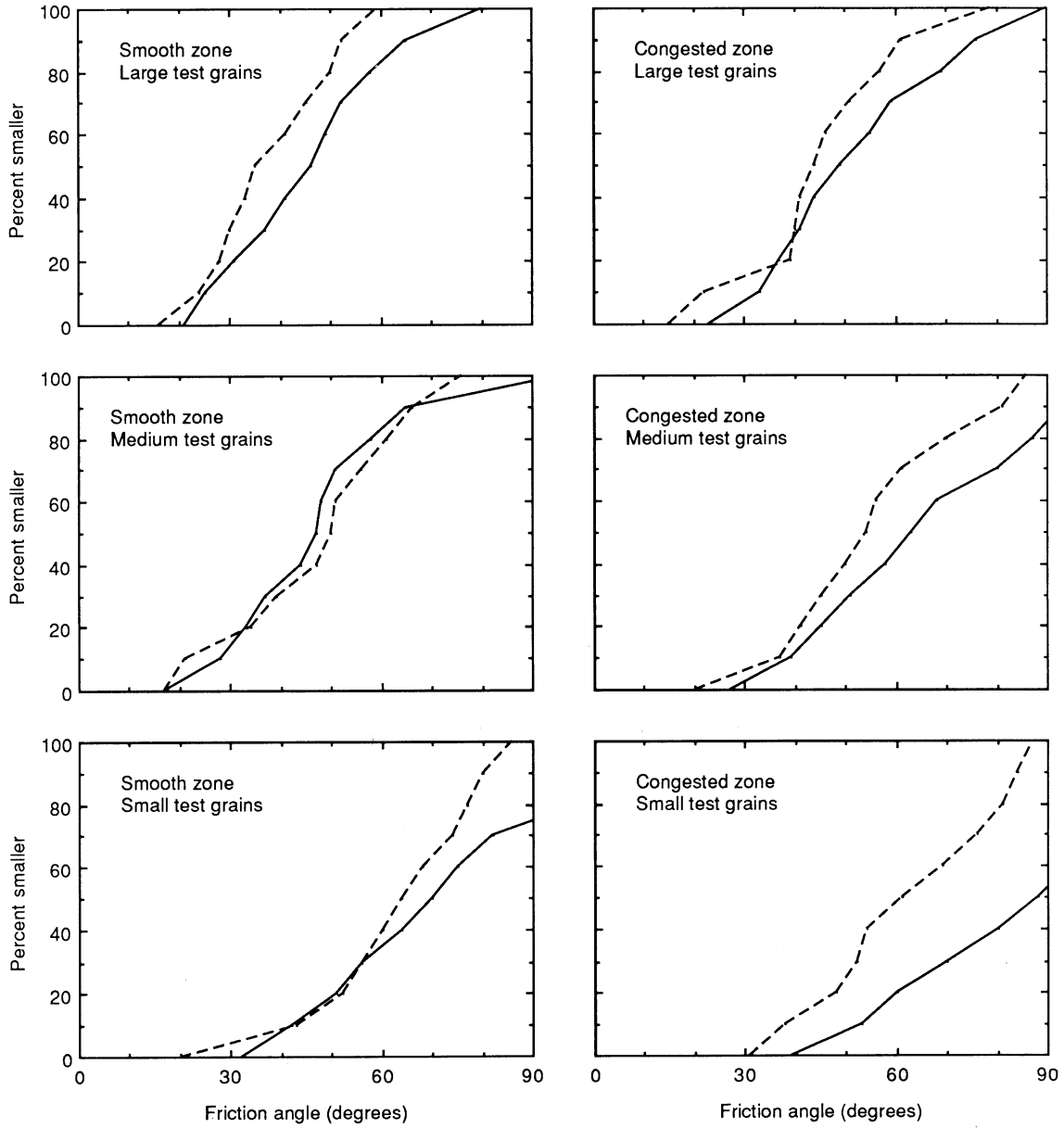

Fig. 10. Comparison of friction angle distributions estimated from bed surface transect profiles with disc-shaped 'grains' (---) and measured with natural grains by tilting (——).

'grains' placed on the profile lack the angularity that contributes to the friction angle of the natural test grains; the difference in friction angles is of the same order as the difference between friction angles measured for spheres and natural grains (Fig. 5). In particular, the discs cannot interlock with the bed, which may account for the relative scarcity of friction angles at the upper end of the range. Secondly, the profiles lack the overhanging topography that traps small grains and accounts for the large fraction of friction angles over 90° in the congested zone.

As would be expected, grain protrusion, as measured by projection and exposure, varies markedly with both grain size and packing geometry (Fig. 11). Larger grains project further above the surface and have greater exposure above upstream obstacles, both directly because they are larger, and indirectly because their size makes them less likely to fall into gaps between other grains. This latter effect is, of course, more pronounced in the congested zone where such pores are larger and more common. The relative difference in grain projection and exposure between the two bed surfaces increases with decreasing grain size. Note in particular that nearly half of the small grains in the congested zone do not project above the mean bed at all, and nearly all are sheltered by large grains upstream (exposure <0). These grains are largely lost to the flow, except for small-scale eddies within their pockets.

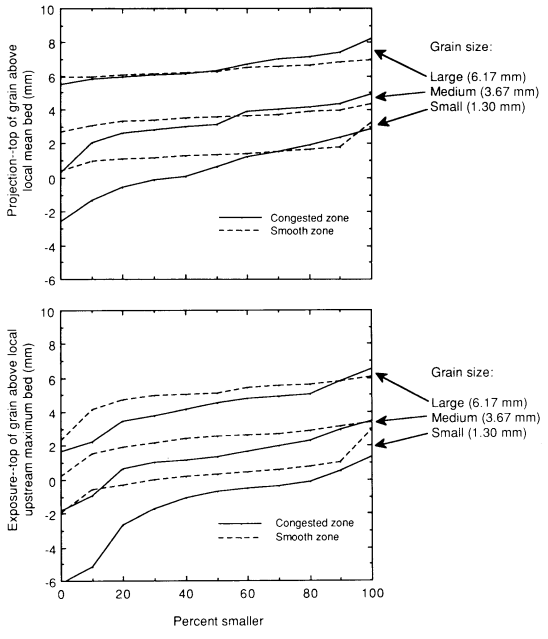

Fig. 11. Distribution of grain projection and exposure estimated from bed surface transect profiles.

Grain protrusion may be considered to be measured by projection, exposure, or both. Median grain projection (p) is approximately equal to the diameter of the grain of interest; the regression relationship $p_{50}=1{\cdot}11\ D-0{\cdot}15\ K_{50}$ ($r^2>0{\cdot}9$) describes nearly all the variation among the six median protrusion values in Fig. 11. Median grain exposure (e), by contrast, is more clearly a function of both the bed grain size and the grain size of interest; the regression relationship $e_{50}=1{\cdot}01\ D-0{\cdot}43\ K_{50}$ ($r^2>0{\cdot}9$) holds for our data. Many of the fines on a poorly sorted bed may have negative exposure values.

Geometric arguments based on an idealized grain packing scheme (Fig. 12) lead to the conjecture that friction angle, grain exposure and projection should be directly related to one another by the expressions (see also Wiberg & Smith, 1987a):

$$e=\tfrac{1}{2}[D-K_{50}+(D+K_{50})\cos\Phi],\ p=e+\frac{\pi}{12}K_{50} \quad (5)$$

(where it is assumed that the median is representative of the grain size of the bed). In fact, however, measurements on the bed surface profiles show almost no relationship between the friction angle and protrusion of individual grains, for a given bed type and grain size (Fig. 13). Perhaps surprisingly, for a given bed and grain size there is only a weak correlation between projection and exposure values for individual grains of a particular size (Fig. 14). Projection and exposure are better correlated *between* the clusters of points representing different grain sizes; these correlations are driven by the obvious fact that, all else equal, larger grains will protrude higher into the flow.

The lack of correlation between projection and exposure among individual pockets on a bed is outwardly counterintuitive. However, projection is

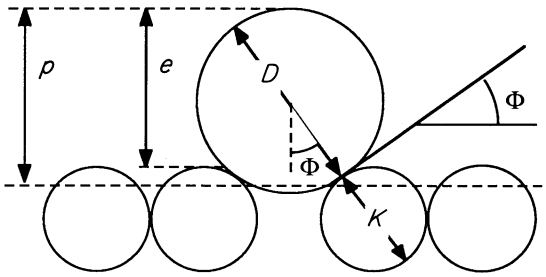

Fig. 12. Idealized geometry for calculating grain projection (p) and exposure (e) as a function of grain sizes (D and K) and friction angle (Φ) (see Eqs 5 and 6).

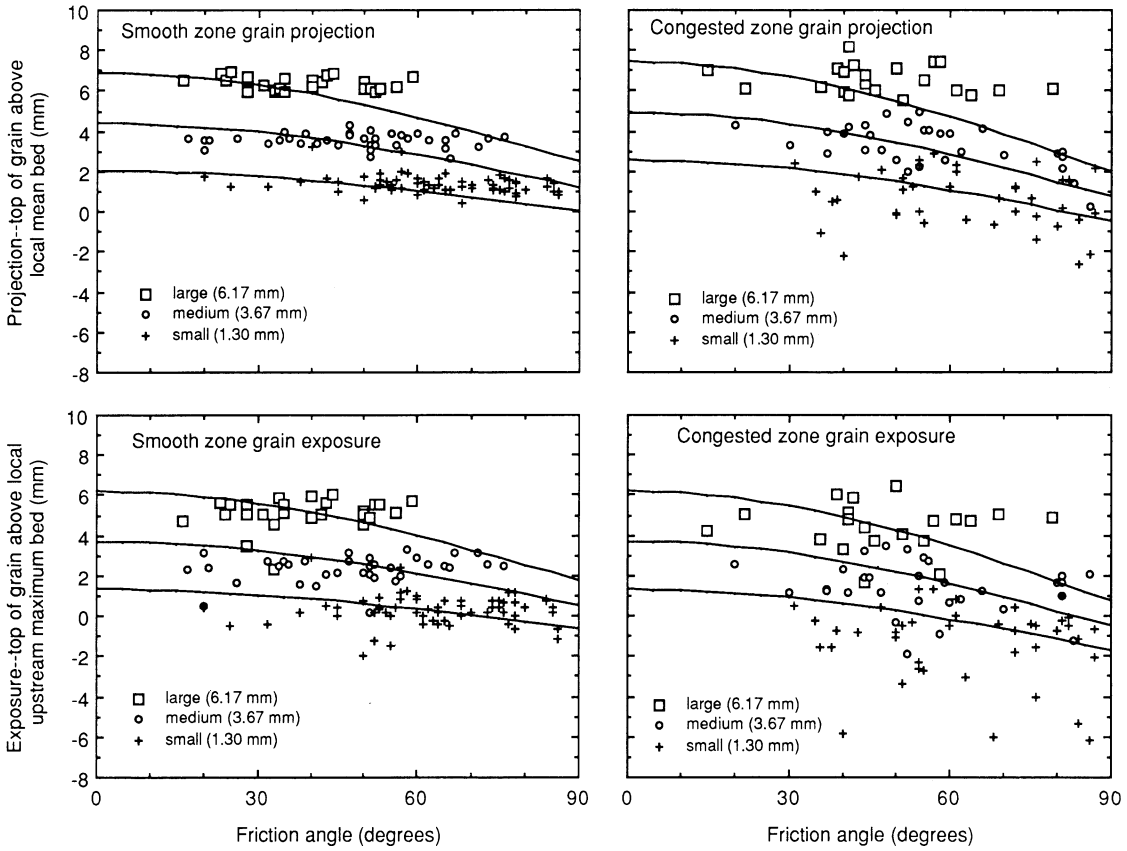

Fig. 13. Projection and exposure measured for individual grains on bed surface transect profiles, as a function of grain friction angle. Curves show relationship expected from idealized geometry (Eq. 5).

defined with respect to the local mean bed, and exposure is measured relative to the local upstream maximum; these reference levels need not be well correlated. Inspection of the autocovariance spectra for both surfaces reveals that the standard deviation of successive points separated by a distance of K_{84} (the length scale used to define exposure and projection) is 90% of the standard deviation of the elevation data as a whole. In other words, points K_{84} apart on the transects will be nearly as uncorrelated as points chosen at random.

To a first approximation, these data suggest that the friction angle, projection, and exposure of individual grains could be modelled as interrelated statistical distributions of independent stochastic variables. Thus, it is necessary to predict only the statistical distributions of projection and exposure, rather than their values for individual grains. From Eq. (5), we can develop the following expression for the nth percentiles of the exposure and projection distributions:

$$e_n = \tfrac{1}{2}[D - K_{50} + (D + K_{50}) \cos \Phi_{100-n}],$$

$$p_n = e_n + \frac{\pi}{12} K_{50}. \quad (6)$$

This relationship quite accurately predicts representative percentiles of the measured projection and exposure distributions (Fig. 15), although errors that appear small may, for small grains, represent a large fraction of the grain diameter. We emphasize that the geometry underlying Eq. (6) does not hold for individual grains (Fig. 13). In other words, for example, the e_{90} for a collection of grains of a specified size can be estimated from their Φ_{10}, even though any individual grain with a friction angle of $\Phi \approx \Phi_{10}$ is unlikely to have an exposure of $e \approx e_{90}$. Despite its seemingly mechanistic basis, therefore, Eq. (6) is strictly empirical.

Directly measuring grain projection, exposure and friction angle, as performed here, is tedious; there is an obvious need for procedures for inferring these

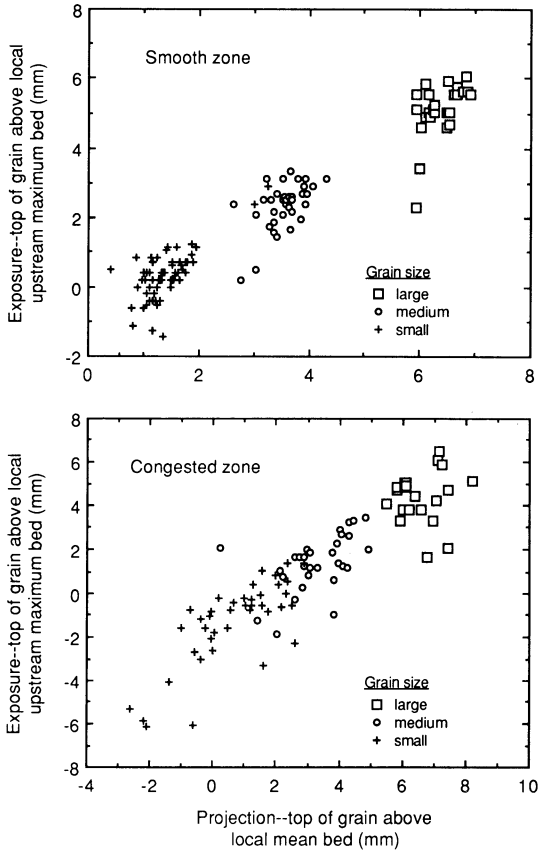

Fig. 14. Correlation of projection and exposure measurements for individual idealized spherical grains, from bed surface transect profiles.

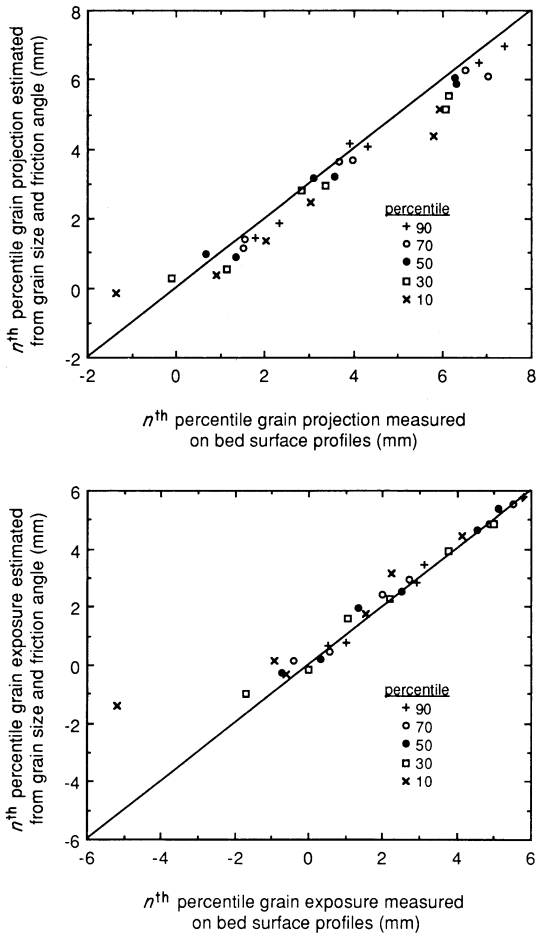

Fig. 15. Representative percentile values of grain projection and exposure, calculated from grain sizes and friction angle distribution (Fig. 10) using Eq. (6), compared to measured projection and exposure distributions (Fig. 11) for idealized spherical 'grains' on bed surface transect profiles.

distributions from more easily measured quantities. Given only the median grain size of the bed surface, Eq. (4) might be used to estimate friction angle distributions for different grain sizes, which, in turn, could be used in Eq. (6) to infer projection and exposure distributions. We offer two caveats concerning this approach. First, we have defined projection and exposure in essentially arbitrary ways, which may not accurately characterize the interaction of grains and the flow. Secondly, because our equations are inherently phenomenological, their range of validity is unknown. We have tested them with only very limited data representing only a subset of the bed textures and grain shapes encountered in other circumstances. Uncritical extrapolation of these results to other domains carries obvious risks. To define workable proxy measures of grain exposure and projection, further quantitative study of sediment surface topography is needed.

VARIABILITY IN CRITICAL SHEAR STRESS

How does the variability in friction angle and grain protrusion within a given bed surface affect the variation in critical shear stress among the grains on a bed? A complete answer to this question must await a detailed understanding of turbulent flow near rough boundaries. The approach here is necessarily more modest. Using a relatively simple analytical model for the force balance on individual bed grains, calculations are made of the critical shear stress of each of the idealized spherical 'grains' for which individual friction angle and grain protrusion measurements

were obtained from the bed surface profiles of the two zones described above.

Our approach is a simplification of that developed by Wiberg & Smith (1987a). First, we consider the force balance at the threshold of motion for an individual spherical grain of diameter D (see Fig. 1):

$$\frac{F_D}{\tan\Phi}+F_L=F_W=\tfrac{1}{6}(\rho_s-\rho)g\pi D^3, \tag{7}$$

where F_D and F_L are the drag and lift forces, respectively, exerted on the grain by the flow, F_W is the immersed weight of the grain, g is gravitational acceleration, and ρ_s and ρ are the density of the sediment and the fluid, respectively (for these calculations $\rho_s=2{\cdot}65$ g cm^{-3} and $\rho=1$ g cm^{-3}). The fluid's lift and drag on the grain are functions of the flow velocity. Because the flow is hydraulically rough, the mean flow velocity will be a logarithmic function of distance above the bed:

$$u(z)=\sqrt{\tau_b/\rho}\,\kappa^{-1}\ln\left(\frac{z+z_0}{z_0}\right), \tag{8}$$

where τ_b is the boundary shear stress, van Karman's constant is $\kappa=0{\cdot}407$, z_0 is a length scale proportional to the roughness length scale of the bed, and z is defined such that $z=0$ at the reference height where $u=0$. (It is usual to define z such that $z=z_0$ where $u=0$; under this convention, the argument of the logarithm in Eq. (8) would be z/z_0. We use our convention because it simplifies the analysis which follows.) There is no universally accepted procedure for defining the value of z_0 for poorly sorted sediments. Here, while conceding that bed texture (which determines hydraulic roughness) is not a well-defined function of any particular grain size of the bed, we assume $z_0=K_{84}/10$ in the interest of consistency with the available empirical data (Dietrich & Whiting, 1989). Theoretically, the logarithmic profile is only valid at distances more than approximately $100\,z_0$ above the bed, well above the region of interest for this analysis. Near the bed, the flow is complicated by the wakes of individual grains, and the velocity profile may be expected to vary from place to place. There is an urgent need for a more complete understanding of the flow field close to rough beds. However, measurements by Grass (1971) suggest that the logarithmic profile holds well below $100\,z_0$, and Einstein (1950, p. 12) mentions measurements that show that it even holds down to $z=3\,z_0$ (i.e. below the tops of the grains). In the interests of simplicity, we extend the logarithmic profile down to $z=0$, and write:

$$u(z)=\sqrt{\tau_b/\rho}\,\kappa^{-1}f(z),$$
$$\text{where}\quad f(z)=\ln\left(\frac{z+z_0}{z_0}\right)\quad z\geq 0 \qquad f(z)=0\quad z\leq 0. \tag{9}$$

We assume that the reference height $z=0$ is the local mean bed elevation, taken as the average bed over a distance of K_{84} upstream and downstream of the grain (which is also the reference level for our measurements of grain projection).

Since the grain Reynolds number is high, the drag force can be expressed as the integral of the impact-law drag over the exposed surface of the grain:

$$F_D=\frac{C_D}{2}\rho\int_{p-e}^{p}w(z)u(z)^2\,dz$$
$$=\frac{C_D}{2}\frac{\tau_b}{\kappa^2}\int_{p-e}^{p}\sqrt{D^2-[2z-(2p-D)]^2}\,f(z)^2\,dz, \tag{10}$$

where C_D is an empirically determined drag coefficient, $w(z)$ is the width of the grain cross-section, p is the elevation of the top of the grain (i.e. projection) above the local mean bed, and e is the exposure of the grain (see above). Thus, $p-e$ is the lowest level of the grain exposed to the flow. Similarly, we can express the lift force as

$$F_L=\frac{C_L}{2}\rho A[u(p)^2-u(p-D)^2]$$
$$=\frac{C_L}{8}\frac{\tau_b}{\kappa^2}\pi D^2[f(p)^2-f(p-D)^2], \tag{11}$$

where C_L is an empirically determined lift coefficient and A is the plan view cross-sectional area of the grain. Values of 0·4 for C_D and 0·2 for C_L are assumed (Wiberg & Smith, 1985).

By definition, the critical shear stress τ_{cr} is the boundary shear stress τ_b that imposes sufficient lift and/or drag on a given grain to satisfy the force balance in Eq. 7. Therefore, the preceding equations can be solved to express the critical shear stress as

$$\tau_{cr}=(\rho_s-\rho)g(\pi D^3/6)\left\{\frac{1}{\tan\Phi}\frac{C_D}{2\kappa^2}\right.$$
$$\times\int_{p-e}^{p}\sqrt{D^2-[2z-(2p-D)]^2}\,f(z)^2\,dz$$
$$\left.+\frac{\pi C_L}{8\kappa^2}D^2[f(p)^2-f(p-D)^2]\right\}^{-1} \tag{12}$$

This expression can be recast in dimensionless form by scaling the critical shear stress (τ_{cr}), vertical axis (z), and grain projection and exposure (p and e) by

grain diameter (D), and in turn scaling the grain diameter (D) by z_0, so that:

$$\tau_{cr}^* = \frac{\tau_{cr}}{(\rho_s - \rho)gD} \qquad D^* = \frac{D}{z_0} \approx \frac{10D}{K_{84}}$$

$$z^* = \frac{z}{D} \qquad p^* = \frac{p}{D} \qquad e^* = \frac{e}{D},$$

whereby the dimensionless form of Eq. (12) becomes

$$\tau_{cr}^* = \left[\left[\frac{1}{\tan\Phi}\frac{3C_D}{\pi\kappa^2}\int_{p^*-e^*}^{p^*} \sqrt{1-[2z^*-(2p^*-1)]^2} \times [\ln(z^*D^*+1)]^2\, dz^* + \frac{3C_L}{4\kappa^2}\{[\ln(p^*D^*+1)]^2 - [\ln(p^*D^*-D^*+1)]^2\}\right]\right]^{-1}, \quad (13)$$

where it is understood that the logarithm of an argument less than 1 will be assumed zero.

Dimensionless critical shear stress is strongly dependent on grain protrusion, friction angle, and grain diameter in relation to bed roughness (Fig. 16). Friction angle variations of $\pm$15–20° above and below typical median values (roughly a range of two standard deviations) account for roughly a twofold variation in dimensionless critical shear stress. Similarly, grains with 70–100% of their diameters projecting above $z=0$ (again, roughly two standard deviations, although both mean projection and its variance vary with both D and K) span a twofold dimensionless shear stress range. Note that dimensionless critical shear stress also decreases markedly with increasing dimensionless grain diameter (D^*), even when dimensionless projection (p^*), exposure (e^*) and friction angle are held constant. This reflects the fact that as grain diameter increases with respect to the roughness length scale of the bed, the grain protrudes further up the logarithmic velocity profile, into faster flow.

Because critical shear stress is strongly dependent on friction angle and grain protrusion, which vary substantially from point to point within a rough bed, such beds would be expected to exhibit a wide distribution of critical shear stresses. We can directly estimate the width of this distribution for the idealized spheres for which we have measured individual values of friction angle, projection, and exposure from the bed surface profiles shown in Figs 6 and 9. Using Eq. (12) and these measurements, the critical shear stress for each grain is calculated and the values aggregated to form critical shear stress distributions for the bed surfaces (Fig. 17).

Critical shear stresses estimated for these individual spherical grains on the bed profiles vary substantially (Fig. 17). This variation increases systematically with increasing bed roughness and with decreasing grain size, reflecting the greater friction angle and protrusion variability of smaller grains and rougher beds. For a given grain size on a given bed, the 90th percentile critical shear stress is at least two or three times greater than the 10th percentile. Even for a given grain size on a given bed, therefore, the critical shear stress is a wide distribution rather than a single value. For example, the standard deviation of this distribution is approximately twice the difference in median critical shear stresses between the two surfaces, for either large or medium grains.

These calculations necessarily depend on assumptions (particularly concerning the character of the near-bed flow field) that may not be realistic, and which cannot be verified at present. The validity of Eq. (12) as a predictor of critical shear stress is untested, and the specific critical shear stress values derived here should not be treated uncritically. Our primary purpose, however, was to estimate the variability in critical shear stresses, rather than their exact values; the robustness of these two kinds of estimates will be governed by different factors. The calculations underlying Fig. 17 may underestimate the shear stress variation of natural grains because, by assuming the test grains are spheres, they ignore the variability of shape between individual grains and the variability of orientation of an individual grain in an individual pocket. Alternatively, if the velocity gradient near the local mean bed elevation $z=z_0$ is actually shallower than a logarithmic profile would indicate (Wiberg & Smith, 1987b), the effect of grain protrusion on critical shear stress (and thus the variability of critical shear stress) would be smaller than suggested here.

The mean boundary shear stress measured in the flume run in which these surfaces were formed (53 dyne cm^{-2}) falls on the extreme lower tail of the calculated critical shear stress distributions. We made no effort to fit the parameters in this analysis to observed critical shear stresses for comparable grain sizes. Our calculations may tend to overestimate the critical shear stress, although it seems unlikely that they are in error by a factor of two or three. Alternatively, if the calculations are approximately realistic, they suggest that critical shear stress, as conventionally measured, is defined by the most mobile grains (those with the lowest friction angles and highest exposures and projections), most likely

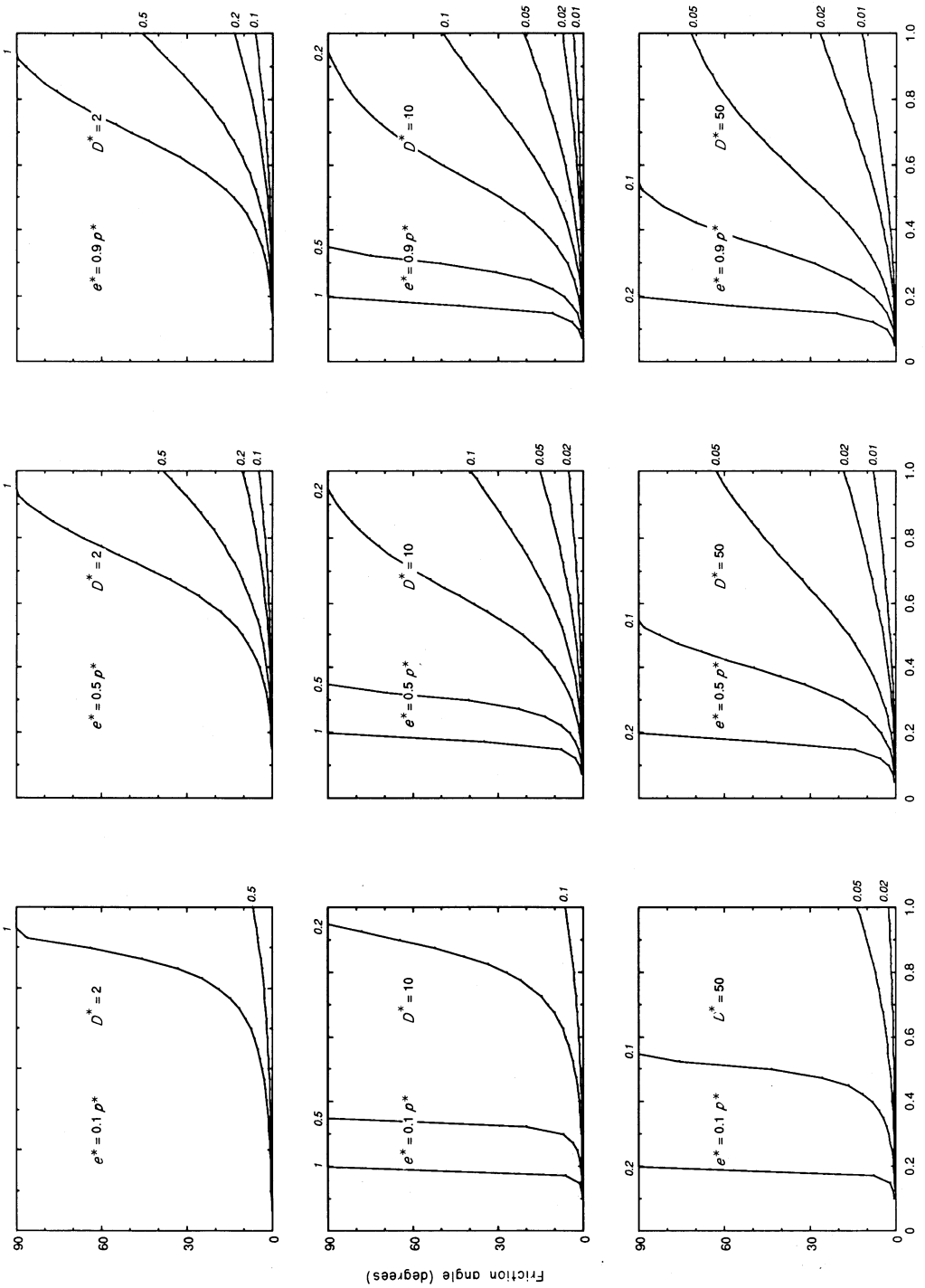

Fig. 16. Contour plots of dimensionless critical shear stress $\tau_{cr}{}^*$, estimated using Eq. (13) ($\tau_{cr}{}^*$ values for each contour in italics), as a function of grain projection and friction angle, for a range of values of dimensionless grain diameter $D^* = D/z_0 = 10\,D/K_{84}$ and exposure/projection ratio e^*/p^*. The ratio e^*/p^* expresses the fraction of the grain protruding above $z = 0$ that is exposed to the flow, rather than shielded by upstream grains.

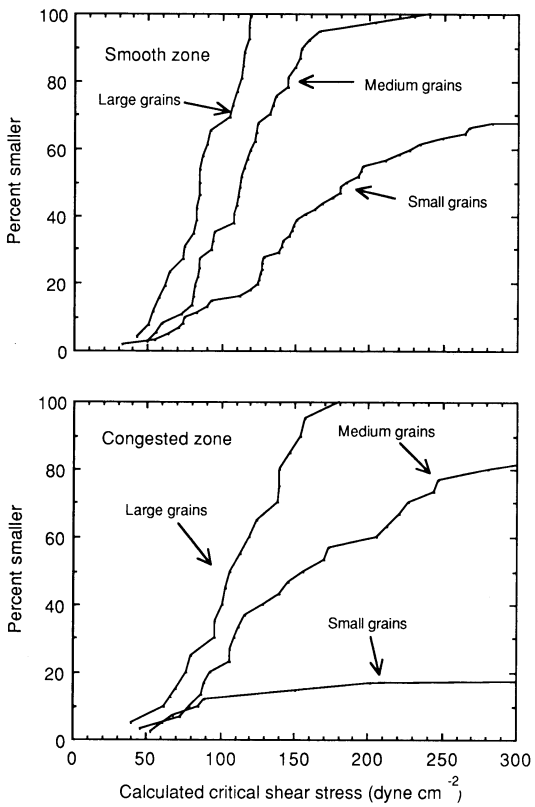

Fig. 17. Critical shear stress (Eq. 12) distribution for spherical grains calculated from individual friction angle, projection, and exposure values (Fig. 13) measured for large (6·17 mm), medium (3·67 mm), and small (1·30 mm) idealized 'spheres' on congested and smooth zone bed surface profiles.

mobilized during transient shear stress excursions associated with sweeps.

DISCUSSION

Efforts to predict and explain sediment transport phenomena have taken different forms. One approach has described the relationships between different variables phenomenologically, by documenting correlations between measured transport rates, flow velocities, grain sizes, etc. Another approach has attempted to understand sediment transport processes, in order to explain the observed correlations and predict these relationships outside the limited range of the available empirical data. One current focus of mechanistic sediment transport studies is the detailed interaction of individual grains on the bed surface with the near-bed flow. Our results suggest that an important issue to be addressed, as such analyses strive for greater detail and realism, is the variability *within* (as distinct from *between*) bed surfaces.

The surface topography of water-worked sediments is complex (Fig. 6). Consequently, friction angle (Fig. 4), grain protrusion (Fig. 11), and estimated critical shear stress (Fig. 17) vary widely among individual grains, even for a single grain size on a single bed surface. Thus, individual grains may have greatly varying entrainability, depending on their exact location on the bed.

These observations are of obvious relevance to efforts to characterize initial motion or selective entrainment thresholds, because they present a clear physical basis for arguing that strict thresholds may not exist. Instead, for example, initial motion may be operationally defined as occurring whenever transient high-velocity local excursions of the turbulent flow are sufficient to move an observable, but small, number of grains representing a given (presumably small) percentile of the critical shear stress distribution (Parker, Dhamotharan, & Stefan, 1982; Wilcock & Southard, 1988).

Because this approximate lower bound of the critical shear stress distribution may be very different from its median or mean, it is unclear whether the erodibility of 'average' grains is reflected in, or measured by, critical shear stresses determined from initial motion studies. Thus, while critical shear stresses (for example, of different grain sizes on a mixed bed) may be operationally defined and phenomenologically estimated, interpreting such results physically is difficult. Which part of the critical shear stress distribution is being measured? Consider, for example, how dimensionless critical shear stress varies with the ratio of grain diameter to the median grain size of the bed (Fig. 18) for the two beds analysed in Fig. 17. The 'equal mobility' hypothesis (Parker & Klingeman, 1987) holds that dimensionless critical shear stress and grain size ratio are inversely proportional, and thus that the log–log plot shown in Fig. 18 should have a slope of -1 (though such a relationship could also arise artefactually, since D appears on the horizontal axis and $1/D$ appears on the vertical). Note that the different percentiles of the distribution have different slopes (the convergence of the regression lines reflects the fact, discussed above, that critical shear stress variability increases with bed roughness and decreases with the grain size of interest). More importantly, operational definitions of critical shear stress may

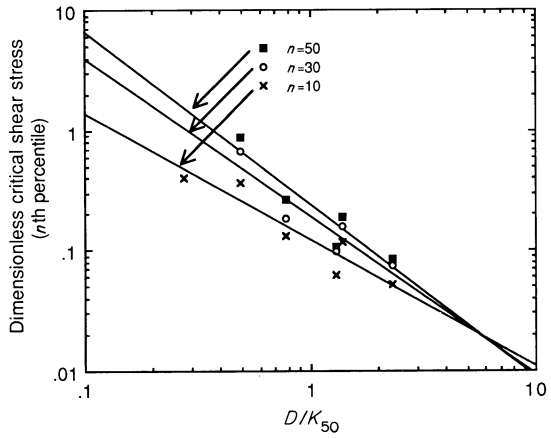

Fig. 18. Dimensionless critical shear stress for selected fractions of the critical shear stress distributions shown in Fig. 17.

measure different percentiles of the underlying distribution for different grain sizes. It is therefore possible to generate a wide range of regression slopes through plots like Fig. 18, if higher percentiles of the distribution are sampled at smaller grain sizes or vice versa.

Recent physically based theoretical treatments of critical shear stress (Wiberg & Smith, 1987a) and flow competence (Komar & Li, 1988) have used the mean or median friction angle as the relevant resistance variable, and mean protrusion as the relevant parameter describing exposure to the flow. It is unclear whether these average values are relevant to threshold situations where 'average' grains will not move, and only those with the lowest critical shear stress will do so. Our results suggest that sediment transport well above initial motion thresholds can occur at a mean boundary shear stress that exceeds critical shear stresses for only a few percent of the grains.

Since turbulent fluctuations in the flow will produce spatial and temporal variations in the applied shear stress, any particular mean boundary shear stress represents a distribution of the probability that, at a given instant, the local shear stress will exceed the critical shear stress for a specific grain (Einstein, 1950). It may therefore be possible to predict the bedload transport rate from a convolution of the probability distributions of instantaneous local shear stress (as a function of mean boundary shear stress) and local critical shear stress (as a function of mean critical shear stress). We are currently exploring this possibility. By inspection, however, it is clear that as the average shear stress increases, turbulent sweeps sufficient to move a given grain will occur more frequently. Conversely, sweeps occurring with a given frequency will be able to move a larger fraction of the bed grains of any given size as the average shear stress increases. These mechanisms may help to explain how bedload transport rates vary with mean boundary shear stress.

Some current sediment transport analyses assume that the 'excess' shear stress (i.e. beyond critical for the bed) is balanced by a momentum defect created by saltating grains, and that this equilibrium controls sediment transport rates (Owen, 1964; Wiberg & Rubin, 1989). That is, for a given applied stress, the transport rate will rise until the momentum defect is sufficient to absorb the excess shear stress. Such a mechanism should be present, and may be particularly important at high transport rates. However, our analysis suggests that at low transport rates, a major factor controlling transport should be the relative scarcity of readily erodible grains on the bed and, equivalently, the relative rarity of sweep events sufficient to move many grains. Thus, the dominant control of transport rates may be the increasing numbers of grains that become available for transport with increasing mean shear stress, rather than a momentum defect balance.

On both of the surfaces analysed, the critical shear stress distributions for each grain size have, within the precision of the estimate, the same lower bound (Fig. 17); this helps to explain the common observation that all grain sizes typically become mobile at nearly the same shear stress. The middle and upper parts of the distributions, however, diverge rapidly. Smaller grains have higher median critical shear stresses and thus lower erodibility. When each large grain moves, however, it may mobilize smaller grains in at least three ways: (i) by evacuating its pocket it changes the friction angles of the smaller grains surrounding it and removes the sheltering effect of its wake on the grains downstream; (ii) its removal implies a local reduction in fluid drag and an increase in near-bed flow velocity; (iii) it may dislodge smaller grains through momentum exchange as it collides with the bed.

Owing to differences in size and mass, these relationships are asymmetrical, i.e. erosion of the coarser fractions tends to mobilize the fines, while the erosion of fines probably inhibits the entrainment of coarse grains (except where the coarse grains are buried by fines). In zones where fines are rare, deposition of fines may mobilize coarse grains by smoothing the bed, thereby increasing the fluid stresses

on the most protruding grains and decreasing their friction angles (Ikeda & Iseya, 1987). Many bed surfaces may therefore be controlled by the equilibrium between the presence of coarse grains inhibiting the entrainment of fines, and the presence of fines mobilizing coarse grains. These conjectures contrast with the 'equal mobility' hypothesis (Parker & Klingeman, 1982) which holds that the coarse surface layer results from the need, as a condition of equilibrium, for the coarser grains to be more numerous on the bed to compensate for their supposed inherently lower mobility. Instead, we suggest that bed surface textures and grain size distributions may be understood in terms of grain interaction mechanisms which control the mobility of each size fraction within an imposed flow and sediment supply regime.

If, as our results suggest, each grain's immediate environment on the bed controls its erodibility, the variability of individual locations on the bed should strongly influence (and be influenced by) many grain interaction and sorting processes. For example, if a few large grains come to rest close to one another (on a surface like that of the smooth zone analysed here), they will locally increase the critical shear stress of all grains by increasing friction angles and decreasing grain protrusion (creating, in effect, a small area whose surface more closely resembles the congested zone). Locally, then, the probability of entrainment will decrease and the probability of distrainment will increase, more coarse grains may be trapped, and a longitudinal sediment sorting into mobile zones of differing textures (Iseya & Ikeda, 1987; Whiting *et al.*, 1988) may result.

In the critical shear stress distributions calculated here (Fig. 17), substantial fractions of the medium and small grains have very high critical shear stresses, and thus very low erodibility. The chance of these grains moving under normal circumstances is small. These results are consistent with field studies using painted rocks, which suggest that some of the tagged particles remain in their original positions, even after repeated floods which exceed the average critical shear stress of all grain sizes (Carling, 1987). While these rocks will undoubtedly move at some point, their low erodibility indicates that the entire bed does not become mobile during an individual flood event, and thus suggests that the wide variations in critical shear stress reported here are reflected in the field as well.

It would be impractical to make detailed measurements of bed surface microtopography, grain protrusion, and friction angle, as a part of every sediment transport study. If only a phenomenological description of the relationship between variables such as applied shear stress, bedload transport rate, and grain size distributions of the bedload and bed is required, intermediate factors such as protrusion and friction angle may perhaps be safely ignored. However, if a mechanistic understanding of the processes governing sediment transport is required, these factors demand attention, by virtue of their role in controlling grain mobility. A more complete understanding of the processes controlling bed surface texture, and, in turn, its impact on sediment transport mechanics, must await a more systematic analysis than that presented here.

SUMMARY

We analysed sediment beds formed in flume experiments at equilibrium with different feed rates of poorly-sorted sediment. Friction angle measurements on the beds led to the following conclusions.

(1) The friction angle Φ of a single grain size on a fixed rough bed is a probability distribution, rather than a single characteristic value. The 10th and 90th percentiles of friction angle on a single bed span an average range of roughly 45°, approximately three times the range of variation among the median friction angles of the water-worked beds studied.

(2) For grains that are small compared to the median bed grain size, substantial fractions of the friction angle measurements exceed 90°. Many of these grains are effectively lost to the flow for long periods.

(3) A water-worked bed and an unworked bed of comparable grain size distribution had markedly different friction angle distributions. Median friction angles for three grain sizes were (in order of decreasing grain size) 3, 20, and 40° greater on the artificial bed than on the water-worked bed. Friction angle values from previous analyses using artificially constructed beds may not be applicable to the water-worked beds of natural sediments, due to differences in packing geometry between the two types of surfaces.

(4) The empirical formula $\bar{\Phi}=\alpha(D/\bar{K})^{-\beta}$ proposed by Miller & Byrne (1966) appears to hold, although no consistent relationships between α and grain shape, or β and grain size sorting, were observed. The empirical relationship can be

generalized to $\Phi_n = (30 + 0{\cdot}5n)\ (D/K_{50})^{-0{\cdot}3}$ to describe friction angle distributions on the water-worked beds studied, for percentiles between $n = 10$ and $n = 70$.

We estimated two measures of grain protrusion above the bed—the level of the grain relative to the vertical velocity profile of the flow, termed 'projection', and its level relative to shielding by upstream grains, termed 'exposure'—by placing idealized disc-shaped grains on microtopographic profiles surveyed along streamwise transects across two bed surfaces of widely differing texture. These analyses suggest the following.

(5) The complex, disordered microtopography of sediment surfaces bears little resemblance to the more orderly grain arrangements often shown in the sediment transport literature, or the evenly spaced uniform roughness elements typically assumed in the fluid dynamics literature.
(6) Grain projection and exposure are characterized by probability distributions that vary markedly with grain size and bed texture. Projection, exposure, and friction angle values for individual grains are poorly correlated, suggesting that these three variables can be modelled as independent stochastic distributions.
(7) The distributions of exposure and projection for a given grain size can be estimated from its friction angle distribution and the median bed grain size, using the empirical relationships $e_n = \frac{1}{2}[D - K_{50} + (D + K_{50}) \cos \Phi_{100-n}]$ and $p_n = e_n + (\pi/12)K_{50}$, derived from idealized grain packing geometry.

Using a force balance analysis (Wiberg & Smith, 1987a) and our friction angle and grain protrusion measurements, we estimated the critical shear stresses of individual idealized spherical grains. This analysis suggests the following.

(8) Critical shear stress is strongly dependent on grain projection, exposure, and friction angle, all of which vary from point to point within a water-worked bed. Therefore, the critical shear stress of a single grain size on a rough bed is not a single value, but instead a probability distribution which becomes broader with decreasing grain size and increasing bed roughness. Thus, distinct initial motion or selective entrainment thresholds may not exist.
(9) In flume experiments, significant sediment transport took place on the analysed surfaces at mean boundary shear stresses that fell on the extreme lower tails of the calculated critical shear stress distributions. Thus, transport well above initial motion thresholds may occur when most grains cannot be entrained by the mean flow, and can only be mobilized by transient shear stress excursions associated with sweeps.
(10) On each surface, the critical shear stress distributions for the three grain sizes analysed have approximately the same lower bound; this provides a physical explanation for the common observation that all grain sizes typically become mobile at nearly the same mean shear stress.
(11) On water-worked, poorly sorted beds, smaller grains tend to have lower grain protrusion and higher friction angles, and therefore higher critical shear stresses and lower erodibility than larger grains, above the lower tails described in (10). Some grains have very high critical shear stresses, and probably remain immobile for long periods.
(12) We speculate that the rapid rise in bedload transport rate observed with increasing boundary shear stress may result from the mobilization of an increasing number of more resistant grains, residing in deeper pockets, with higher friction angles and lower protrusion.

The large variability in critical shear stress, even for a single grain size, points to the need to reconsider how best to model the mechanics of bedload transport and sediment sorting. The use of a single critical shear stress value for a given grain size would now seem inappropriate for many purposes. A theory encompassing the effects of both turbulent fluctuations in instantaneous boundary shear stress applied by the flow, and critical shear stress variation among individual grains, would be a promising step in the development of mechanistic approaches to sediment transport.

ACKNOWLEDGMENTS

This paper resulted from a collaboration originating in a bilateral research project sponsored by the U.S. National Science Foundation and the Japan Society for the Promotion of Science. The experiments reported here were performed at the Environmental Research Center of the University of Tsukuba, and were supported by the Ministry of Education, Science,

and Culture (Grant-in-Aid for Scientific Research 62460235). We thank Yoshinori Kodama and Hideo Iijima for their assistance, and Peter Whiting, Zhenlin Li, and an anonymous reviewer for their comments. J.W.K. thanks the University of California, the American Geophysical Union, and the William and Flora Hewlett Foundation for financial support; this work was also partially supported by NSF 84-51175 to W.E.D.

REFERENCES

BAGNOLD, R.A. (1941) *The Physics of Blown Sand and Desert Dunes*. Methuen, London, 265 pp.

DU BOYS, M.P. (1879) Études du regime et l'action exercée par les eaux sur un lit à fond de graviers indefinement affouilable. *Ann. Ponts Chaussées*, 5, **18**, 141–195.

CARLING, P.A. (1987) Bed stability in gravel streams, with reference to stream regulation and ecology. In: *River Channels: Environment and Process* (Ed. by Richards, K. S.), pp. 321–347. Basil Blackwell, Ltd, Oxford.

CHEPIL, W.S. (1959) Equilibrium of soil grains at the threshold of movement by wind. *Proc. Soil Sci. Soc.*, **23**, 422–428.

DIETRICH, W.E., KIRCHNER, J.W., IKEDA, H. & ISEYA, F. (1989) Sediment supply and the development of the coarse surface layer in gravel-bedded rivers. *Nature*, **340**, 215–217.

DIETRICH, W.E. & WHITING, P.J. (1989) Boundary shear stress and sediment transport in river meanders of sand and gravel. In: *River Meandering* (Ed. by Ikeda, S. & Parker, G.), pp. 1–50. American Geophysical Union, Washington: AGU Water Resources Monograph No. 12.

EAGLESON, P.S. & DEAN, R.G. (1961) Wave-induced motion of bottom sediment particles. *Trans. Am. Soc. civ. Engrs*, **126: 1**, 1162–1186.

EINSTEIN, H.A. (1950) The bed load function for sediment transportation in open channel flows. *Technical Bulletin No. 1026*, U.S. Department of Agriculture, Washington, D.C., 71 pp.

FENTON, J.D. & ABBOTT, J.E. (1977) Initial movement of grains on a stream bed: the effect of relative protrusion. *Proc. R. Soc. A*, **352**, 523–527.

FURBISH, D.J. (1987) Conditions for geometric similarity of coarse stream-bed roughness. *Math. Geol.*, **19**, 291–307.

GRASS, A.J. (1971) Structural features of turbulent flow over smooth and rough boundaries. *J. Fluid Mech.*, **50**, 233–255.

IKEDA, H. & ISEYA, F. (1987) Thresholds in the mobility of sediment mixtures. In: *International Geomorphology 1986 Part I* (Ed. by Gardiner, V.) pp. 561–570. Wiley, London.

ISEYA, F. & IKEDA, H. (1987) Pulsations in bedload transport rates induced by a longitudinal sediment sorting: a flume study using sand and gravel mixtures. *Geogr. Annlr*, **69**, 15–27.

KELLERHALS, R. & BRAY, D.I. (1971) Sampling procedures for coarse fluvial sediments. *J. Hydraul. Div. Am. Soc. civ. Engrs*, **97**, 1165–1180.

KOMAR, P.D. & LI, Z. (1986) Pivoting analyses of the selective entrainment of sediments by shape and size with application to gravel threshold. *Sedimentology*, **33**, 425–436.

KOMAR, P.D. & LI, Z. (1988) Applications of grain-pivoting and sliding analyses to selective entrainment of gravel and to flow-competence evaluations. *Sedimentology*, **35**, 681–695.

KUHNLE, R.A. & SOUTHARD, J.B. (1988) Bed load transport fluctuation in a gravel bed laboratory channel. *Wat. Resour. Res.*, **24**, 247–260.

LEOPOLD, L.B., WOLMAN, M.G. & MILLER, J.P. (1964) *Fluvial Processes in Geomorphology*. W. H. Freeman & Co., San Francisco, 522 pp.

LI, Z. & KOMAR, P.D. (1986) Laboratory measurements of pivoting angles for applications to selective entrainment of gravel in a current. *Sedimentology*, **33**, 413–423.

MEYER-PETER, E. & MÜLLER, R. (1948) Formulas for bed-load transport. *Proc. Int. Ass. Hydraulic Research, 3rd Ann. Conf., Stockholm*, 39–64.

MILLER, R.L. & BYRNE, R.J. (1966) The angle of repose for a single grain on a fixed rough bed. *Sedimentology*, **6**, 303–314.

OWEN, P.R. (1964) Saltation of uniform grains in air. *J. Fluid Mech.*, **20**, 242–255.

PAINTAL, A.S. (1971) Concept of critical shear stress in loose boundary open channels. *J. Hydraul. Res.*, **9**, 91–113.

PARKER, G., DHAMOTHARAN, S. & STEFAN, S. (1982) Model experiments on mobile, paved gravel bed streams. *Wat. Resour. Res.*, **18**, 1395–1408.

PARKER, G. & KLINGEMAN, P.C. (1982) On why gravel bed streams are paved. *Wat. Resour. Res.*, **18**,1409–1423.

SHIELDS, A. (1936) Anwendung der Ähnlichkeitsmechanik und der Turbulenzforschung auf die Geschiebebewegung. *Mitt. Preuss. Vers. Anst. Wasserb. Schiffb.*, **36**, 26 pp (translated by W. P. Ott & J. C. van Uchelen, U.S. Department of Agriculture, Soil Conservation Service Coop Laboratory, California Institute of Technology).

WHITING, P.J., DIETRICH, W.E., LEOPOLD, L.B., SHREVE, R.L. & DRAKE, T. (1988) Bedload sheets in heterogeneous sediment. *Geology*, **16**, 105–108.

WIBERG, P.L. & RUBIN, D.M. (1989) Bed roughness produced by saltating sediment. *J. Geophys. Res.*, **94**, 5011–5016.

WIBERG, P.L. & SMITH, J.D. (1985) A theoretical model for saltating grains in water. *J. Geophys. Res.*, **90**, 7341–7354.

WIBERG, P.L. & SMITH, J.D. (1987a) Calculations of the critical shear stress for motion of uniform and heterogeneous sediments. *Wat. Resour. Res.*, **23**, 1471–1480.

WIBERG, P.L. & SMITH, J.D. (1987b) Initial motion of coarse sediment in streams of high gradient. In: *Erosion and Sedimentation in the Pacific Rim* (Ed. by Beschta, R. L., Blinn, T., Grant, G. E., Ice, G. G. & Swanson, F. J.), pp. 299–308. IAHS Press, Wallingford, UK. IAHS Publication No. 165.

WILCOCK, P.R. & SOUTHARD, J.B. (1988) Experimental study of incipient motion in mixed-size sediment. *Wat. Resour. Res.*, **24**, 1137–1151.

WOLMAN, M.G. (1954) A method of sampling coarse river-bed material. *Trans. Am. geophys Union*, **35**, 951–956.

(Manuscript received 21 June 1989; revision received 27 November 1989)

APPENDIX

Symbols used in this paper, and their definitions, are:

A plan-view cross-sectional area of grain
C_D drag coefficient
C_L lift coefficient
D diameter of bedload or test grain (grain analysed for entrainability)
D_b intermediate axial diameter of test grain
D_c smallest axial diameter of test grain
D_n nth percentile of bedload grain size distribution
$D^* = D/z_0$ dimensionless grain diameter
e exposure of top of grain above local upstream maximum bed elevation
e_n nth percentile of grain exposure distribution
$e^* = e/D$ dimensionless grain exposure
f vertical displacement function in mean velocity profile
F_D fluid drag force on grain
F_L fluid lift force on grain
F_W immersed weight of grain
g gravitational acceleration
K diameter of bed surface grain
K_n nth percentile of bed surface grain size distribution
p projection of top of grain above local mean bed elevation
p_n nth percentile of grain projection distribution
$p^* = p/D$ dimensionless grain projection
u streamwise mean flow velocity
w cross-stream width of grain
z vertical displacement
z_0 length scale of logarithmic velocity profile
$z^* = z/D$ dimensionless vertical displacement
α fitted parameter in Eq. (2)
α_n fitted parameter for nth percentile in Eq. (3)
β fitted parameter in Eq. (2)
β_n fitted parameter for nth percentile in Eq. (3)
γ grain pivoting pathway factor in Eq. (1)
Φ friction angle
Φ_n nth percentile of friction angle distribution
κ van Karman's constant, $\kappa \approx 0{\cdot}407$
ρ density of water
ρ_s density of sediment grains
τ_b boundary shear stress
τ_{cr} critical boundary shear stress
$\tau_{cr}^* = \tau_{cr}/[(\rho_s - \rho)gD]$ dimensionless critical shear stress